



GPU Nuclear Corporation  
Post Office Box 480  
Route 441 South  
Middletown, Pennsylvania 17057-0191  
717 944-7621  
TELEX 84-2386  
Writer's Direct Dial Number:

(717) 948-8000

April 8, 1993  
C312-93-2021  
C000-93-2050

Nuclear Regulatory Commission  
Attn: Document Control Desk  
Washington, DC 20555

Three Mile Island Nuclear Station Unit 2 (TMI-2)  
Operating License No. DPR-73  
Docket No. 50-320  
Response to NRC Questions on TMI-2 RV  
Criticality Analyses and Post-Defueling Survey Report

Dear Sir:

NRC letter dated March 22, 1993, requested additional information concerning the TMI-2 Reactor Vessel (RV) Criticality Safety Analysis Report and the TMI-2 RV Post-Defueling Survey Report (PDSR). Enclosure 1 provides a response to each of the seven questions contained therein.

Sincerely,

*R. L. Long*  
R. L. Long  
Director, Corporate Services/TMI-2

140057

EDS/dlb

Enclosures

cc: T. T. Martin - Regional Administrator, Region I  
M. T. Masnik - Project Manager, PDNP Directorate  
L. H. Thonus - Project Manager, TMI  
F. I. Young - Senior Resident Inspector, TMI

9304150042 930408  
PDR ADOCK 05000320  
P PDR

GPU Nuclear Corporation is a subsidiary of the General Public Utilities Corporation

## ENCLOSURE 1

### 1. Criticality Study

"Criticality Safety Analysis Report for the Three Mile Island Unit 2 Reactor Vessel (RV)," R. L. Long to US Nuclear Regulatory Commission, December 18, 1992.

Q1a. The study stated that the fissile material used in the study included uranium with 2.67 wt percent U-235. Did the study also consider Pu, since the fuel had experienced burnup?

A1a. Yes. The fuel composition used in the analyses was burned, batch-3 fuel moderated to the extent required to obtain the highest  $k_{\infty}$  value (i.e., optimal moderation) which included Plutonium. The composition of the burned fuel was obtained using the SAS2 analysis sequence of the SCALE code system (Reference 1). The initial enrichment for batch-3 fuel was 2.96 wt%. The assumed burnup for the batch-3 fuel was 2535 MWd/tonne U and the decay time was 2075 days (3/28/79 - 12/1/84). Table 1 includes the isotopic compositions calculated by SCALE/SAS2 and assumed to be in burned batch-3 fuel. Reference 2 (enclosed) provides more information on the relative reactivity worth of different fuel compositions. In the criticality analyses, when impurities were added to the fuel or the particle sizes were changed, searches were performed to ensure optimum moderation (i.e., highest  $k_{\infty}$  value) conditions were maintained.

#### References:

1. "SCALE: A Modular Code System for Performing Standardized Computer Analyses for Licensing Evaluation," NUREG/CR-0200, Vols. 1-3, U.S. Nuclear Regulatory Commission (originally issued July 1980, reissued January 1982, Rev. 1 issued July 1982, Rev. 2 issued June 1983, Rev. 3 issued December 1984). Code system available from the Radiation Shielding Information Center at Oak Ridge National Laboratory.
2. Cecil V. Parks, Robert M. Westfall, and B. L. Broadhead, "Criticality Analysis Support for the Three Mile Island Unit 2 Fuel Removal Operations," *Nuclear Technology*, 87, 660-678 (1989).

Q1b. The section of the study that dealt with an accidental criticality stated that the fuel available for such a criticality is loose fuel that can be relocated from each reactor vessel zone. The study listed the quantity that would be loose in each zone, but did not explain the methodology by which the value was determined. Additional information is required on how these quantities were determined. Our particular concern is Zone 9, the bottom

Table 1. Nuclide compositions in burned Batch-3 Fuel  
(other than  $\text{UO}_2$ )<sup>a</sup>

Nuclide	Composition (atoms/barn-cm)
Pu-238	8.913-9 <sup>b</sup>
Pu-239	3.527-5
Pu-240	1.761-6
Pu-241	2.188-7
Pu-242	5.145-9
Sm-147	1.066-6
Sm-148	3.866-8
Sm-149	1.006-7
Sm-150	6.288-7
Sm-151	1.788-7
Sm-152	2.865-7
Sm-154	6.014-8
La-139	3.975-6
Ce-140	3.877-6
Ce-142	3.598-6
Ce-144	1.810-8
Eu-151	8.202-9
Eu-152	3.959-11
Eu-153	1.318-7
Eu-154	4.506-9
Eu-155	6.124-9
Pm-147	2.936-7
Nd-143	3.543-6
Nd-145	2.389-6
Nd-146	1.881-6
Nd-148	1.072-6
Pr-141	3.598-6

<sup>a</sup> $\text{U}(2.67)\text{O}_2$  at 10.3 g/cm<sup>3</sup>

<sup>b</sup>8.913E-9 = 8.913 x 10<sup>-9</sup>

head region where the criticality is most likely to occur. Only 59 kg of fuel is assumed to be loose out of 95 kg assumed to be present in this zone. How was this value determined, and what is the justification for considering the other 36 kg as "neutronically decoupled" from the postulated pile of relocated loose fuel?

- A1b. The intent of the accident criticality analysis was to conservatively estimate the amount of residual fuel that could non-mechanistically relocate to the lower head of the RV. The original analysis (References 1 and 2) assumed that all of the loose fuel relocated to the lower head. Since the residual fuel estimates obtained by the passive neutron measurements did not characterize the type of fuel (i.e., loose or resolidified), a ratio of the amount of loose fuel from the earlier analysis to that determined by the passive neutron measurements was used with some modifications. Zones 1 through 4 contain basically all loose fuel; therefore, the passive neutron measurement values for these zones, i.e., 10, 225, 150, and 99 kg, respectively, were used directly. For Zones 5 through 9, a multiplier on loose fuel was calculated based on total new fuel quantities versus original analysis quantities.

Zone 5 was unusual in that the multiplier was 15.25, which was much greater than any other multiplier. However, Reference 3 states that 109.0 kg of the 154.0 kg total is accounted for by extensive crusting of resolidified material on various surfaces. To be conservative, it was assumed that the 109 kg represents the total amount of resolidified material, leaving 45 kg of loose fuel in Zone 5.

Further, the original analysis assumed that all the loose fuel in the annular gap (Zone 6) relocated to the lower head. However, as stated in the NRC PDMS Technical Evaluation Report (Reference 4, pg. 5-7), this material "...would not be available to be redistributed to the lower head." Therefore, the quantity of loose fuel in the annular gap was not included in the analysis.

Zones 7 and 8 primarily contained resolidified fuel; therefore, a straight ratio was used in those zones. Zone 9 extended from the bottom of the Incore Guide Tube Support Plate (IGSP) to and including the lower head, a distance of about 4.7 feet. The "pile" of loose fuel that was postulated to accumulate on the lower head reached a maximum height of less than 8 inches (see Table 4 of the criticality study). Therefore, using the logic that neutronic separation is achieved by approximately 12 inches of water, any residual, non-loose fuel located more than 20 inches vertically from the bottom of the RV is neutronically decoupled from the postulated pile. The fuel from Zone 9 presumed to be available to relocate consisted of: all of the loose fuel located between the IGSP and the flow distributor; all of the fuel on the head surface (this assumption was conservative by approximately 10 kg); 98% of the fuel in the incore instrument nozzles (2% or 0.6 kg was assumed to be distant from the pile); and none of the fuel in the incore instrument guide tubes left suspended from the flow distributor (they are assumed to be located more than 20 inches vertically from the bottom of the RV). Based on this, the calculated

residual fuel contribution from Zone 9 is 58.7 kg.

Please note that although Zone 9 is the area where loose fuel is nonmechanistically assumed to accumulate, the accident criticality calculations prove that no criticality would occur, even considering extremely conservative assumptions. Therefore, contrary to the statement contained in this question (i.e., "...the bottom head region where the criticality is most likely to occur."), criticality will not occur in the bottom head region (or anywhere else for that matter) of the TMI-2 reactor vessel.

Therefore, the total quantity of loose fuel that is assumed to relocate to the lower head is about 620 kg, detailed as follows:

<u>Zone</u>	<u>Loose Fuel (kg)</u>
1	10
2	225
3	150
4	99
5	45
6	28.8
7 & 8	2.6
9	<u>58.7</u>
	<u>619.1 kg</u>

References:

1. GPU Nuclear letter 4410-90-L-0026, "Results of Post-Lower Head Sampling Program Cleanup," dated April 12, 1990.
  2. TMI-2 Defueling Completion Report.
  3. GPU Nuclear calculation 4249-3211-91-019, Rev. 0, "Dry RV Zone 5 Fuel Results," October 1991.
  4. Technical Evaluation of TMI-2 Post-Defueling Monitored Storage, February 1992, transmitted by letter, Michael T. Masnik, NRR, to Dr. Robert L. Long, GPU Nuclear, dated February 20, 1992.
2. Reactor Vessel Post-Defueling Survey Report

"TMI-2 Post-Defueling Survey Report for the Reactor Vessel," R. L. Long to US Nuclear Regulatory Commission, dated February 1, 1993.

Q2a. In the review performed by the "Rasmussen Committee," several biases were ascribed to the passive neutron measurement study. Two of these biases, boron variations and UO<sub>2</sub> particle size, were attributed to zones 1 through 5 only. The Committee reasoned that the biases were restricted to these 5 zones based on the nature of the fuel melting during the accident. A substantial amount of work has occurred inside the reactor since the accident possibly causing a considerable amount of fuel relocation. Provide a justification for the limitation of the biases to zones 1 through 5 that is consistent with what is known about the distribution of fuel debris inside the reactor vessel.

A2a. The passive neutron method employed took advantage of the fact that the uranium and other actinides in spent fuel are alpha ( $\alpha$ ) emitters and some of the  $\alpha$ s bombarding the oxygen atoms in UO<sub>2</sub> undergo an ( $\alpha, n$ ) reaction that produces energetic neutrons. Since the ratio of uranium (U) to oxygen (O) is fixed, the number of neutrons produced by this process is proportional to the amount of uranium. This will be true whether the source is a powder or pellets or a mixture of both. At TMI-2 however, the Reactor Vessel (RV) water contained about 5000 ppm of boron (B) to prevent criticality. Unfortunately,  $\alpha$ s also react with boron to give energetic neutrons. As the vessel was drained, just how much boron was left behind and deposited on surfaces as the water dried is unknown, and thus contributes to the uncertainty of the passive neutron measurement. In addition, the number of neutrons produced by the boron ( $\alpha, n$ ) reaction is greatly affected by the size of the UO<sub>2</sub> particles. The range of an  $\alpha$  particle of this general energy is about 50  $\mu$  ( $1\mu = 10^{-6}$  meters) in water and about 1/10th of that in UO<sub>2</sub>. Thus, in large (>50  $\mu$ ) UO<sub>2</sub> particles, very few of the  $\alpha$ s emitted will get out, but if the UO<sub>2</sub> particles were approximately 1  $\mu$ , essentially all of the  $\alpha$ s would get out of the UO<sub>2</sub> particles and potentially interact with a boron nucleus. Measurements have shown that this effect can be as large as a factor of 100 or more.

Prior to the SNM Measurement Program, a series of rubble samples taken from the RV were analyzed for neutron emission rate. The samples used for calibration are similar in character to the kind of material that remains in the lower half of the RV. Therefore, the passive neutron measurement should give a fairly good measure of the amount of residual fuel (i.e., UO<sub>2</sub>) in that region. In fact, there is excellent agreement between the amount estimated by the original (video) analysis and the amount determined by the passive neutron measurement technique for combined Zones 7 and 8, i.e., 226 kg and 202 kg, respectively. However, there is a relatively small amount of rubble-type material above the midplane of the core. In that region, most of the residual fuel appears to be either fine particles or a thin film deposited on metal surfaces. These finer forms of UO<sub>2</sub> would significantly increase the number of neutrons produced by ( $\alpha, n$ ) reactions on boron, i.e., the neutron measurements would indicate too large an amount of UO<sub>2</sub>.

Most of the fuel remaining in Zones 6 through 9 is similar to the samples used to determine neutron yield. (For Zones 6 and 9, the passive neutron estimate greatly

exceeds the visual estimate, in relative terms, mainly due to the greater surface area in those two zones having a fine dusting of residual fuel.) However, the fuel remaining in Zones 1 through 5 is comprised primarily of fine particles adherent to surfaces since there is very little "visible" fuel debris. Therefore, there is a significant positive bias (i.e., counting rate too high) in Zones 1 through 5. To be conservative, the boron thickness and UO<sub>2</sub> particle size effects were not applied to Zones 6 and 9 although an argument could be made for at least partial inclusion.

- Q2b. The passive neutron study included computer calculations that modeled fuel at positions near the detector and farther from the detector, averaging the two values to arrive at a best estimate. How were the "close" and "far" positions chosen? Was the average of close and far taken as half the distance, or was a more likely "most probable" distance chosen for the averaging?
- A2b. The "close and far positions" were locations where fuel debris was observed in the video tape data from the video inspection effort. Since the video inspection was not considered to be sufficiently quantitative, the video results were only used to select locations where fuel debris could exist in quantity. The largest and smallest quantities of fuel were estimated by locating physically plausible amounts of fuel in the far and near positions, respectively. With the largest and smallest possible quantities defined by this methodology, the midpoint of both analytical results (based on the above assumptions) was selected as the best estimate of fuel debris for a selected zone. Thus, neither the average nor most probable distance was used. The average was the arithmetic average of the calculated fuel quantities using the "close and far" distances.
- Q2c. One of the identified biases was inscattering of neutrons (20 percent). If an inscattering effect occurred, it should be partially accounted for by measurement of neutrons emitted by the calibration source that was lowered near the detector. Explain the justification for assuming that this bias was not accounted for by the use of the neutron source.
- A2c. In the calibration measurement, the detector was placed in the central axis of the RV with the source hanging next to it about 110 cm off the axis. In this case, there is almost no structural material in the vicinity of the source to scatter the neutrons; thus, no in-scatter. Therefore, nearly all of the counts would be due to direct path (i.e., line of sight) neutrons.

Suppose we now count the neutrons from a fuel deposit next to the core baffle plate. A determination of the material located between the source and the detector would be made and the micro-shield computer code would be used to determine the direct path attenuation. The counting rate would be divided by the total attenuation both from geometry and material attenuation to get the number of neutrons from the source. Using the calibration measurement, this would be converted into grams of uranium.

This method would be quite accurate if there were no scattering around the source. In the example, however, the baffle plates are behind the source which would result in the scattering of some neutrons back toward the detector increasing the counting rate. The process would treat the scattered neutrons as though they were emitted toward the detector resulting in too high of a value for the uranium present.

Q2d. In the passive neutron measurement study, was the contribution of neutrons that were emitted by fuel below the waterline considered by the analysis? If so, how?

A2d. This contribution was considered to be small due to neutron attenuation in water (i.e., the slant angle) and other inherent errors associated with the counting system. Therefore, the fuel located below the waterline was not included as a contributor to the neutron flux for a specific zone under consideration.

Q2e. Provide additional detail concerning the nine fuel samples that were measured to determine the neutron emission rate (these samples are now stored at INEL). The masses of uranium in these samples are listed in Table 3 of Calculation Sheet 4249-3211-91-006, Rev. No. 1 (sheet No. 17 of 30). Provide any available report that documents these fuel masses, and any other documentation available about the nature of these samples, especially the physical form (large lumps versus powder), and inclusion of impurities such as steel or boron.

A2e. The data is reported in the following documents which are enclosed:

- 1) GPUNC Technical Bulletin, "R6 and Lower Vessel Debris Final Examination Results," TB-89-12-0, December 1989.
- 2) T. Hardt & G. Hayner, "TMI-2 B-Loop Steam Generator Tube Sheet Loose Debris Examination and Analysis," GEND-INF-090, US DOE, June 1989.
- 3) D. W. Aikers, et al, "TMI-2 Core Debris Grab Samples...Examination and Analysis," GEND-INF-075, Part 1, US DOE, 1986.
- 4) G. Hayner, "TMI-2 H8A Core Debris Sample Examination, Final Report," GEND-INF-060, Vol. II, US DOE, May 1985.

# TMI- 2 TECHNICAL BULLETIN

TB 89-12, Rev. 0  
December 12, 1989  
Page 1 of 13

SUBJECT: R-6 and Lower Vessel Debris Final Examination Results

SUMMARY:

This technical bulletin distributes the attached letter (Reference 1) which reports the results of the analysis of R-6 and lower head core debris samples. The samples were analyzed by EG&G Idaho at the Idaho National Engineering Laboratory (INEL). The results should be considered in conjunction with GEND-INF-084, "Examination of Debris From the Lower Head of the TMI-2 Reactor", and GEND-INF-075, "TMI-2 Core Debris Grab Samples - Examination and Analysis, Part 2".

IMPLICATIONS & USE:

This data may be used for fuel measurement calculations, for the SNM accountability plan, and criticality analysis.

ATTACHMENT:

1. D. W. Ackers. "R-6 and Lower Head Vessel Debris Final Examination Results". EG&G Idaho Memorandum #DWA-43-89 (12 sheets).

REFERENCE:

1. D. W. Ackers. R-6 and Lower Vessel Debris Final Examination. EG&G Memorandum #DWA-43-89. Idaho Falls, ID: EG&G Idaho, Inc.  
17 November 1989.

PREPARED BY: A. P. Kelsey 12/15/89  
A. P. Kelsey / 4054

APPROVED BY: C. H. Distenfeld 12/15/89  
C. H. Distenfeld / 8954

APPROVED BY: D. R. Buchanan 12/15/89  
D. R. Buchanan / 8321

November 17, 1989

Mr. D. R. Buchanan  
GPU Nuclear Corporation  
Box 480  
Middletown, Pennsylvania

R-6 AND LOWER VESSEL DEBRIS FINAL EXAMINATION RESULTS DWA-43-89

Dear Sir:

Attached are the results for the R6 sample analyses (Attachment A) and the lower vessel debris samples (Attachment B). It should be noted that Attachment B contains data for both the lower vessel loose debris and debris adjacent to the lower head of the reactor vessel. Data included are the density, uranium content, enrichment, and gamma ray emitter content. Based upon our previous discussions, this report meets all EG&G agreements to provide data to General Public Utilities on lower head samples.

Examination of the results of the loose debris sample analyses indicates that the debris is similar to the earlier lower vessel loose debris examinations as discussed in GEND-INF 084 - Examination of Debris From the Lower Head of the TMI-2 Reactor. Three of the more recent lower vessel loose debris samples (3, 5, and 7) would be expected to be representative of most of the loose debris as Sample 2 (50 wt% uranium) is composed of a small amount of debris (235 g) and is composed of smaller particle sizes. The average enrichment of the three samples is from 56-65 wt% uranium with an average of 61.5 wt%. In comparison, the loose debris samples discussed in GEND INF-084 had an average uranium content of 65 wt% with a range of 62-69 wt%. Within uncertainties, these samples all have the same uranium content. Also, the fission product concentrations are very similar for both groups of samples including the Sb-125 which has been substantially released from the fuel. The samples from adjacent to the lower head of the reactor have not been included in this comparison as only small probably non representative samples (100 mg) were analyzed. These comparisons suggest that the composition of the debris on the lower head is relatively homogeneous and that the sample analysis results as discussed in GEND INF-084 should be representative of the loose debris present on the lower head of the reactor.

The boron concentrations for the lower vessel debris as listed in GEND INF-084 range from the detection limit to .36 wt% with an average of the real values of 0.1 wt%. As these samples were removed from the interior

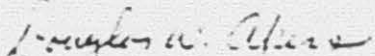
DWA-43-89  
Mr. D. R. Buchanan  
November 17, 1989  
page 2

TB 89-12, Rev. 0  
December 12, 1989  
Page 3 of 13

of particles up to 6 cm in diameter, it is clear that the boron was incorporated into the debris during the accident and was not surface deposited boron. Therefore, the boron content can be considered an integral part of the debris. It should be noted that these observations are based on the samples examined which are not a statistically representative sampling of the debris bed.

If you have any questions please contact me at (208) 526-6118.

Very truly yours,



Douglas W. Akers  
Nuclear Sciences

Attachment: As stated

cc: N. S. Burrell (DOE-ID)

Attachment A

R-6 SAMPLE ANALYSIS RESULTS

Examinations completed on the R-6 samples include weight, density, uranium content, enrichment and gamma ray emitter content for the dissolved samples. The dissolved sample gamma ray emitter results included in this report are expected to be more accurate than the data for the undissolved samples as those results are affected by the weight and density of the sample material. Table A-1 lists the primary physical data and Table A-2 lists the gamma ray emitter content for each sample analyzed. All gamma ray data for the dissolved samples have been decay corrected to April 1, 1987. Comparisons with the ORIGEN2 calculated Ce-144 content (248 microcuries/g) indicate that the samples have near average Ce-144 content within the uncertainties of the the data. It should be noted that most of the Pr-144 have counting uncertainties of 10-20% and that there is a total uncertainty of 20-30% associated with these data.

The uncertainties associated with the various analyses differ based on the analytical method used. The weight and density data have uncertainties ranging from 2-5%. However, the enrichment and uranium content data have uncertainties of 10-15% due to uncertainties in both the measurement and calibration data for the delayed neutron measurement system. It should be noted that the presence of control materials and other fissile material (e.g., Pu-239) can affect the uranium content and enrichment data. The effect of control material would be to reduce the measured enrichment for the samples by a small amount unless large amounts of control material were present. (Elemental analysis of the original lower head samples suggests that little control material is present). The plutonium content has been determined to be insignificant relative to the U-235 content at the burnup of the TMI-2 core.

Table A-1 - PRINCIPAL PHYSICAL DATA FOR THE R-6 DEBRIS SAMPLES

Sample I.D.	Weight (mg)	Density g/cm <sup>3</sup>	Uranium content (% Uranium) <sup>a</sup>	Enrichment (% 235) <sup>a</sup>
R6-1A	468.2	7.1	74	2.4
R6-1B	204.9	--	77	2.4
R6-2A	399.8	7.1	76	2.4
R6-2B	265	--	77	2.6
R6-3A	347.5	6.7	76	2.4
R6-3B	502	--	77	2.3
R6-4A	495.2	7.5	74	2.6
R6-4B	477.8	--	75	2.6

a. Uncertainties for the uranium content and enrichment data are 10%-15%.

IN 89-12, Rev. 0  
December 12, 1989  
Page 5 of 13

**Appendix Table A-2 Gamma Ray Emitter Content for the R-6 Samples  
(microcuries/g on April 1, 1987)**

Sample	27Co-60			45Ru-106			51Cr-125			55Co-134			59Fe-144			63Cu-154						
	Act/B	%	Error	Act/B	%	Error	Act/B	%	Error	Act/B	%	Error	Act/B	%	Error	Act/B	%	Error				
R-6-14	0.7516	00	+/- 1.22E-01	00	0	+/- 0.000E+00	00	+/- 0.000E+00	00	3.78E-01	+/- 1.12E-01	+/- 1.12E-01	1.64E-01	+/- 3.37E-02	+/- 3.37E-01	1.51E+01	+/- 3.9E+00	+/- 3.9E+01				
R-6-19	0.1511	00	+/- 1.11E-01	00	0	+/- 0.000E+00	00	3.61E-01	+/- 1.19E-01	+/- 1.19E-01	1.62E-01	+/- 3.30E-02	+/- 3.30E-01	1.64E-01	+/- 3.4E-02	+/- 3.4E-01	1.64E+01	+/- 3.4E+00	+/- 3.4E+01			
R-6-28	0.4515	00	+/- 1.16E-01	00	0	+/- 0.000E+00	00	3.32E-01	+/- 1.65E-01	+/- 1.65E-01	1.66E-01	+/- 3.02E-02	+/- 3.02E-01	1.66E-01	+/- 3.2E-02	+/- 3.2E-01	1.66E+01	+/- 3.2E+00	+/- 3.2E+01			
R-6-79	0.1877	00	+/- 1.17E-01	00	0	+/- 0.000E+00	00	+/- 0.000E+00	00	3.50E-01	+/- 1.62E-01	+/- 1.62E-01	1.63E-01	+/- 3.02E-02	+/- 3.02E-01	1.63E-01	+/- 3.4E-02	+/- 3.4E-01	1.63E+01	+/- 3.4E+00	+/- 3.4E+01	
R-6-34	0.6646	00	+/- 9.09E-02	00	0	+/- 0.000E+00	00	7.31E-01	+/- 3.48E-01	+/- 3.48E-01	1.77E-01	+/- 2.99E-02	+/- 2.99E-01	1.77E-01	+/- 3.1E-02	+/- 3.1E-01	1.77E-01	+/- 3.4E-02	+/- 3.4E-01	1.77E+01	+/- 3.4E+00	+/- 3.4E+01
R-6-39	7.4645	00	+/- 9.77E-02	00	0	+/- 0.000E+00	00	6.41E-01	+/- 3.30E-01	+/- 3.30E-01	1.63E-01	+/- 2.45E-02	+/- 2.45E-01	1.63E-01	+/- 2.6E-02	+/- 2.6E-01	1.63E-01	+/- 2.8E-02	+/- 2.8E-01	1.63E+01	+/- 2.8E+00	+/- 2.8E+01
R-6-44	1.0008	01	+/- 1.04E-01	00	0	+/- 0.000E+00	00	4.81E-01	+/- 2.11E-01	+/- 2.11E-01	1.24E-01	+/- 1.66E-02	+/- 1.66E-01	1.24E-01	+/- 1.8E-02	+/- 1.8E-01	1.24E-01	+/- 2.0E-02	+/- 2.0E-01	1.24E+01	+/- 2.0E+00	+/- 2.0E+01
R-6-48	0.3141	00	+/- 6.92E-02	00	0	+/- 0.000E+00	00	4.56E-01	+/- 2.81E-01	+/- 2.81E-01	1.61E-01	+/- 1.35E-02	+/- 1.35E-01	1.61E-01	+/- 1.7E-02	+/- 1.7E-01	1.61E-01	+/- 1.9E-02	+/- 1.9E-01	1.61E+01	+/- 1.9E+00	+/- 1.9E+01

Attachment B

LOWER VESSEL DEBRIS ANALYSIS RESULTS

Examination of data from the lower vessel loose debris and the hard material adjacent to the lower head have been completed. The following data are included in this attachment:

- Table B-1 - Density and particle size of the lower vessel debris  
Table B-2 - Uranium enrichment and content for the lower vessel debris  
Table B-3 - Gamma ray emitter content for the lower vessel loose debris solid samples

The uncertainties associated with the various analyses differ based on the analytical method used. The weight and density data have uncertainties ranging from 2-5%. However, the enrichment and uranium content data have uncertainties of 10-15% due to uncertainties in the measurement and calibration data for the delayed neutron measurement system. Other uncertainties associated with the uranium content and enrichment measurements are addressed in the footnote to Table B-2.

The solid sample gamma ray spectrometry data listed in Table B-3 are not corrected for mass attenuation by the sample mass. Therefore, the solid sample data are approximate and the results are most accurate for those samples whose radionuclide content is calculated using gamma ray energies greater than 1.0 MeV (primarily Co-60 and Pr-144). Mass attenuation corrections can be applied to obtain better information for the low energy gamma ray emitters (i.e., Ru-106, Sb-125, Cs-134, and Cs-137). These gamma spectrometry data have associated uncertainties of 20-30% for the high energy gamma ray emitters.

Table B-1 - PARTICLE SIZE AND DENSITY FOR THE LOWER VESSEL DEBRIS

<u>Particle size</u>	Particle size distribution (%)/ (Density g/cm <sup>3</sup> )			
	SSC-1-2	SSC-1-3	SSC-1-5	SSC-1-7
>4 mm	6.5 (8.0)	36.6 (7.2)	37.2 (7.8)	26.6 (7.6)
2-4 mm	13.8 (7.8)	33.7 (7.3)	26.5 (8.2)	37.3 (7.8)
1-2 mm	11.6 (6.3)	18.9 (7.6)	16.7 (8.0)	23.6 (7.8)
710-1000 <sup>a</sup> micron	5.9 (4.6)	4.6 (8.8)	4.8 (8.0)	4.6 (7.9)
300-710 micron	16.1 (6.3)	4.9 (8.1)	8.5 (7.7)	5.2 (6.5)
150-300 micron	14.5 (5.7)	0.91 (8.1)	3.2 (7.7)	1.4 (6.5)
90-150 micron	11.2 (6.5)	0.17 (4.6)	1.3 (7.2)	0.52 (7.2)
38-90 micron	13.4 (6.3)	0.07 (3.8)	1.1 (6.4)	0.48 (4.4)
<38 micron	7.0 (4.1)	--	0.72 (4.0)	0.28 (3.8)
Weighted Average Densities	6.3	7.4	7.9	7.7

a. Densities below a particle size of 710 micron have uncertainties of 50% because of the small amount of material measured.

Table B-1 cont'd

<u>Sample I.D.</u>	<u>Density (g/cm<sup>3</sup>)</u>
SSC 1-8	7.7
SSC 1-9	9.4
SSC 1-10	6.9
SSC 1-11	8.6
SSC 1-12	8.2

---

a. Densities based on the analysis of several gram samples.

Table B-2 - URANIUM CONTENT AND ENRICHMENT FOR THE LOWER VESSEL DEBRIS<sup>a</sup>

<u>Particle size</u>	<u>Uranium content (%) / [Enrichment %]</u>			
	SSC-1-2	SSC-1-3	SSC-1-5	SSC-1-7
>4 mm	68 (2.4)	62 (2.6)	73 (2.7)	69 (2.4)
2-4 mm	48 (2.6)	45 (2.8)	-	64 (2.6)
1-2 mm	49 (--b)	62 (2.7)	43 (2.7)	65 (2.8)
710-1000 <sup>a</sup> micron	47 (2.6)	58 (2.6)	50 (2.6)	56 (2.5)
300-710 micron	51 (2.9)	53 (2.4)	51 (2.8)	58 (2.6)
150-300 micron	-	58 (2.6)	56 (2.6)	50 (2.4)
90-150 micron	50 (2.6)	53 (2.4)	54 (2.6)	52 (2.8)
38-90 micron	41 (2.3)	54 (2.8)	52 (2.5)	64 (2.4)
<38 micron	46 (--b)	--	--	55 (2.5)

Table B-2 cont'd

<u>Sample I.D.</u>	<u>Uranium content(%)<sup>a</sup></u>	<u>Enrichment (%)</u>
SSC 1-8	65	2.6
SSC 1-9	27	2.3
SSC 1-10	48	2.7
SSC 1-11	70	2.4
SSC 1-12	62	2.7

a. Uncertainties are 10-15% for both uranium content and enrichment data. Also, it should be noted that the presence of control materials and other fissile material (e.g., Pu-239) can affect the uranium content and enrichment data. The effect of control material would be to reduce the measured enrichment for the samples by a small amount unless large amounts of control material were present. (Elemental analysis of the original lower head samples suggests that little control material is present). The plutonium content has been calculated to be insignificant relative to the U-235 content for the burnup of the TMI-2 core.

b. Measured enrichments higher than the 2.98% maximum in the core are indicated for these samples. However within a 2 sigma uncertainty, the data are within acceptable limits. A review of these data was performed to assess possible errors in the calculations or measurements. No errors were found.

**Appendix Table B-3 Gamma Ray Mitter Content for the Lower Vessel Samples**  
**(Solid samples - Not corrected for mass attenuation)**  
**(Microcuries/g on April 1, 1987)**

Sample I-D.		Weight of Sample (grams)		270±50		550±134		550±137		630±134		630±134		630±134		630±134		
Description & Item Fractions		LC1/0	Error	LC1/0	Error	LC1/0	Error	LC1/0	Error	LC1/0	Error	LC1/0	Error	LC1/0	Error	LC1/0	Error	
BD-13C-1-2A																		
4mm	0.4382	4.0758±00	+/-	1.1161±01	+/-	2.6564±01	+/-	7.1171±02	+/-	4.4841±00	+/-	3.8571±01	+/-	6.5154±01	+/-	0.0004±00	+/-	3.0731±01
2mm	0.2141	3.4624±00	+/-	8.2046±02	+/-	7.9031±00	+/-	1.4311±01	+/-	3.4331±02	+/-	1.9584±00	+/-	2.8151±01	+/-	3.4064±01	+/-	1.9464±02
1mm	0.2093	4.9234±00	+/-	1.0708±01	+/-	1.6331±01	+/-	2.2014±01	+/-	0.4841±02	+/-	5.3111±00	+/-	1.4511±01	+/-	2.4796±01	+/-	2.7844±01
110um	0.2198	5.0004±01	+/-	3.8061±01	+/-	1.5264±01	+/-	2.0451±01	+/-	7.6021±02	+/-	8.8358±00	+/-	2.2531±01	+/-	3.3941±01	+/-	0.0004±00
300um	0.2173	4.6154±01	+/-	7.4084±01	+/-	2.6104±01	+/-	5.0631±01	+/-	1.3821±01	+/-	8.9834±00	+/-	2.7194±01	+/-	6.8471±01	+/-	0.0004±00
110nm	ND	+/-	0.0000±00	+/-	ND	+/-	0.0000±00	+/-	ND	+/-	0.0000±00	+/-	ND	+/-	0.0000±00	+/-	0.0000±00	
90nm	0.2031	3.7098±01	+/-	5.4711±01	+/-	3.6104±01	+/-	1.8844±01	+/-	3.8144±00	+/-	2.8411±01	+/-	7.9001±01	+/-	8.0196±01	+/-	0.0001±00
35nm	0.1902	8.2727±01	+/-	5.7004±01	+/-	2.1198±01	+/-	3.8127±01	+/-	1.0351±03	+/-	2.7631±00	+/-	3.1118±01	+/-	8.2764±00	+/-	0.0004±00
Bottom Pan	0.2677	1.4228±01	+/-	1.6134±01	+/-	6.4604±00	+/-	9.4009±02	+/-	3.1104±02	+/-	1.9234±00	+/-	5.1691±00	+/-	7.0725±01	+/-	0.0004±00
BD-13C-1-3A																		
4mm	0.2674	5.7041±00	+/-	1.4634±01	+/-	2.6421±01	+/-	5.7304±02	+/-	2.0631±00	+/-	3.2684±01	+/-	4.4038±01	+/-	0.0004±00	+/-	3.7311±01
2mm	0.2079	1.9344±01	+/-	3.2724±01	+/-	1.1621±01	+/-	2.4534±01	+/-	4.9046±02	+/-	1.1784±00	+/-	2.4794±01	+/-	9.2568±01	+/-	4.0274±01
1mm	0.2047	6.9348±00	+/-	1.2424±01	+/-	6.7271±00	+/-	1.4448±01	+/-	2.8511±02	+/-	1.0264±00	+/-	3.7408±01	+/-	9.3661±01	+/-	2.8074±01
110um	0.2894	6.4844±01	+/-	5.3194±01	+/-	2.1064±01	+/-	4.0008±01	+/-	1.0311±03	+/-	2.2731±00	+/-	3.0034±01	+/-	3.4114±01	+/-	3.9771±01
300um	0.2222	7.5394±01	+/-	5.9171±01	+/-	1.8834±01	+/-	1.7511±02	+/-	6.4064±00	+/-	2.5534±01	+/-	3.1954±01	+/-	0.0004±00	+/-	5.8554±01
110nm	0.2619	4.9834±01	+/-	7.2724±01	+/-	3.1334±01	+/-	1.5724±03	+/-	8.7284±01	+/-	7.8484±01	+/-	0.0002±00	+/-	0.0002±00		
90nm	0.2137	5.9044±01	+/-	3.0951±01	+/-	2.3104±01	+/-	1.1614±03	+/-	7.4514±00	+/-	1.7454±01	+/-	3.2174±00	+/-	0.0004±00		
35nm	0.2606	5.1894±01	+/-	7.2631±01	+/-	3.6344±01	+/-	1.5471±03	+/-	7.5434±01	+/-	1.4784±01	+/-	2.9071±01	+/-	0.0004±00		

Appendix Table B-3 cont'd

Sample 1-0, Weight Of Sample (gram)			27C-60			33C-134			33C-137			63C-134			63C-136			59P-144		
			Lc1/a	+/ -	Error	Lc1/b	+/ -	Error	Lc1/c	+/ -	Error	Lc1/d	+/ -	Error	Lc1/e	+/ -	Error	Lc1/f	+/ -	Error
BD-1SC-1-5A	0.2940	9.7211E+00	+/ -	1.6431E+01		00	+/ -	0.000E+00	8.1511E+00	+/ -	1.6234E+01	3.9771E+01	+/ -	6.3741E+01	9.8741E+01	+/ -	3.2194E+00	2.040E+02	+/ -	3.3871E+01
Bottom Pan		00	+/ -	0.000E+00		00	+/ -	0.000E+00	00	+/ -	0.000E+00	00	+/ -	0.000E+00	00	+/ -	0.000E+00	00	+/ -	0.000E+00
100mL	0.2775	1.4500E+01	+/ -	2.9051E+01		00	+/ -	0.000E+00	1.2427E+01	+/ -	1.2271E+01	1.0434E+01	+/ -	2.279E+01	5.1048E+01	+/ -	8.000E+00	00	+/ -	0.000E+00
100mL	0.2749	7.5751E+01	+/ -	8.8431E+01		00	+/ -	0.000E+00	2.5308E+01	+/ -	5.3441E+01	2.4026E+01	+/ -	9.1134E+00	2.5451E+01	+/ -	6.2108E+01	00	+/ -	0.000E+00
100mL	0.2744	5.8151E+01	+/ -	6.4031E+01		00	+/ -	0.000E+00	2.5108E+01	+/ -	2.8904E+01	1.2708E+01	+/ -	2.2121E+00	2.4771E+01	+/ -	5.1574E+00	00	+/ -	0.000E+00
100mL	0.2825	5.1250E+01	+/ -	6.1951E+01		00	+/ -	0.000E+00	3.6071E+01	+/ -	5.6546E+01	1.6941E+01	+/ -	6.7746E+00	2.4219E+01	+/ -	5.9508E+01	00	+/ -	0.000E+00
100mL	0.2744	5.5010E+01	+/ -	4.2911E+01		00	+/ -	0.000E+00	3.6441E+01	+/ -	4.4144E+01	1.5004E+01	+/ -	9.7894E+00	2.5021E+01	+/ -	6.0032E+01	00	+/ -	0.000E+00
100mL	0.2951	6.1894E+01	+/ -	4.5360E+01		00	+/ -	0.000E+00	3.1171E+01	+/ -	5.9271E+01	1.5340E+01	+/ -	9.5345E+00	2.4341E+01	+/ -	4.9164E+01	00	+/ -	0.000E+00
Bottom Pan		00	+/ -	0.000E+00		00	+/ -	0.000E+00	00	+/ -	0.000E+00	00	+/ -	0.000E+00	00	+/ -	0.000E+00	00	+/ -	0.000E+00
BD-1SC-1-7A	0.3044	9.1051E+00	+/ -	1.0471E+01		00	+/ -	0.000E+00	1.8121E+01	+/ -	2.7984E+01	0.0011E+02	+/ -	3.9504E+00	3.9728E+01	+/ -	9.3164E+01	00	+/ -	0.000E+00
Bottom Pan	0.1610	5.3100E+00	+/ -	1.2702E+01		00	+/ -	7.6448E+00	1.0508E+01	+/ -	1.0508E+01	1.2634E+02	+/ -	9.4434E+01	2.8294E+01	+/ -	6.7378E+01	00	+/ -	0.000E+00
100mL	0.2111	5.8750E+00	+/ -	1.3727E+01		00	+/ -	6.1536E+00	1.6602E+01	+/ -	1.6602E+01	2.6744E+02	+/ -	1.9121E+00	3.7638E+01	+/ -	4.2536E+01	00	+/ -	0.000E+00
100mL	0.2656	4.9740E+01	+/ -	6.2042E+01		00	+/ -	0.000E+00	2.2911E+01	+/ -	4.1104E+02	2.2772E+00	+/ -	4.9744E+01	9.2134E+01	+/ -	3.9164E+00	00	+/ -	0.000E+00
100mL	0.2617	2.9640E+01	+/ -	3.8934E+01		00	+/ -	1.3538E+01	2.5821E+01	+/ -	6.5534E+02	1.1863E+01	+/ -	3.2131E+01	6.1766E+01	+/ -	3.7774E+00	00	+/ -	0.000E+00
100mL	0.2548	3.2868E+01	+/ -	6.5700E+01		00	+/ -	2.8521E+01	6.8484E+01	+/ -	1.4227E+01	9.2134E+01	+/ -	9.2134E+01	2.2164E+01	+/ -	6.5220E+01	00	+/ -	0.000E+00
100mL	0.2779	2.6424E+01	+/ -	4.6322E+01		00	+/ -	1.5794E+01	3.4164E+01	+/ -	0.1164E+02	5.4011E+00	+/ -	1.0484E+01	4.2748E+01	+/ -	6.3728E+01	00	+/ -	0.000E+00
100mL	0.1720	5.1194E+01	+/ -	6.5404E+01		00	+/ -	1.7011E+01	5.2827E+01	+/ -	1.0511E+01	6.4741E+01	+/ -	6.4571E+01	4.4231E+00	+/ -	6.4421E+00	00	+/ -	0.000E+00
Bottom Pan	0.1913	4.9208E+01	+/ -	6.0444E+01		00	+/ -	2.0245E+01	1.8111E+01	+/ -	2.7121E+01	2.8027E+01	+/ -	3.1751E+00	4.1194E+01	+/ -	6.3001E+01	00	+/ -	0.000E+00

IB 89-12, Rev. 0  
December 12, 1989  
Page 13 of 13

Appendix Table B-3 cont'd

Sample I.B. Description & Size fractions	Weight of sample (g/mm)	27Co 40		55Cr 134		55Cr 137		63Cu 154		43Ca 104		59Fe 164		
		Δε/ε	Error	Δε/ε	Error	Δε/ε	Error	Δε/ε	Error	Δε/ε	Error	Δε/ε	Error	
IB-SIC-1-B4 (one 1 piece)	0.2671	9.0231e+00	+/- 1.9311e-01	2.098e+01	+/- 3.252e-01	9.0471e+01	+/- 1.9008e+02	+/- 3.7731e+01	+/- 1.7771e+01	+/- 3.9101e+01	+/- 1.9111e+00	+/- 0.0004e+00	+/- 1.4848e+02	+/- 4.8404e+01
IB-SIC-1-B4 (two 2 pieces)	0.2818	7.4721e+01	+/- 6.1841e-01	1.6421e+00	+/- 1.8711e-01	6.4271e+01	+/- 8.2004e-01	1.3291e+01	+/- 2.3004e-01	3.9101e+01	+/- 3.1011e+00	+/- 0.0004e+00	+/- 6.1871e+01	+/- 1.8034e+01
IB-SIC-1-B5 (one 1 piece)	0.2893	2.5751e+01	+/- 1.7001e-01	8.4391e+00	+/- 1.2221e+01	1.9491e+01	+/- 5.2131e+00	2.6911e+01	+/- 2.6101e+01	1.9234e+01	+/- 1.3844e+00	+/- 1.9994e+02	+/- 3.0021e+01	+/- 3.0021e+01
IB-SIC-1-B5 (two 2 pieces)	0.4990	4.0941e+00	+/- 8.5971e-02	1.7671e+00	+/- 1.7651e-01	6.6331e+01	+/- 3.5151e+01	4.3071e+01	+/- 5.4341e+01	1.3774e+02	+/- 0.0004e+00	+/- 2.1751e+01	+/- 2.1751e+01	+/- 2.1751e+01
IB-SIC-1-B6 (one 1 piece)	0.3537	8.4651e+00	+/- 1.4741e-01	2.6121e+00	+/- 1.0841e-01	1.1031e+01	+/- 8.7191e-01	4.1701e+01	+/- 6.2121e+01	1.1031e+02	+/- 0.0004e+00	+/- 1.5071e+02	+/- 2.1751e+01	+/- 2.1751e+01

# CRITICALITY ANALYSIS SUPPORT FOR THE THREE MILE ISLAND UNIT 2 FUEL REMOVAL OPERATIONS

CECIL V. PARKS, ROBERT M. WESTFALL, and  
B. L. BROADHEAD *Martin Marietta Energy Systems, Inc.*  
*Nuclear Engineering Applications Department*  
*P.O. Box 2008, Oak Ridge, Tennessee 37831*

Received October 17, 1988

Accepted for Publication April 4, 1989

*Beginning in 1984, the Three Mile Island Unit 2 Defueling Design Team requested Oak Ridge National Laboratory to supply criticality safety analyses in support of the licensing activities for all fuel removal operations. The computational methods and basic analytic models employed in the work are discussed, the areas where computational analyses were requested are reviewed, and the pertinent results are tabulated and discussed.*

## INTRODUCTION

Because of uncertainty in the core configuration, the Three Mile Island Unit 2 (TMI-2) Criticality Task Force decided early in 1984 to use a simple bounding approach for ensuring subcriticality during fuel removal operations. Since that time, staff of the Nuclear Engineering Applications Department at Oak Ridge National Laboratory (ORNL) have supplied criticality safety analysis expertise to the defueling operations. Staff from Bechtel North American Power Corporation worked with the Criticality Task Force and the Defueling Design Team to determine the physical systems requiring a criticality safety analysis. The ORNL staff then worked with Bechtel to determine the appropriate bounding computational model for each analysis. This paper presents the analytic models that were used. Reference 1 provides a more detailed discussion of the physical relevance of the systems modeled and the programmatic significance of the results.

Modules and cross-section data from the SCALE computational system<sup>2</sup> were used for all analyses. The required analyses included resonance cross-section processing, infinite fuel lattice calculations, depletion calculations, Monte Carlo criticality calculations for

multidimensional systems, and discrete ordinates calculations for one-dimensional finite systems. This paper discusses the computational methods and describes the application of each module pertinent to the TMI-2 analyses. The modules were utilized to do the following:

1. develop and characterize an acceptable analytic model for the lower vessel rubble
2. establish safe operating limits for the soluble boron in the reactor coolant system (RCS)
3. establish the limits on foreign materials allowed in the RCS
4. assess the criticality safety related to using a plasma arc torch in removing the lower core support assembly
5. perform parametric criticality analyses for containers with removed core material.

This paper provides details on the analyses performed and the results obtained in each area.

## ANALYSIS METHODS

### Computational Tools

The SCALE computational system was developed for the U.S. Nuclear Regulatory Commission by the Nuclear Engineering Applications Department at ORNL. The SCALE system is modular in structure and enables a user to easily perform a variety of neutronic and thermal analyses by proper back-to-back execution of well-established functional modules. In addition, easy-to-use control modules have been developed to automate and standardize analytic sequences. Using a simplified, free-form input format, a user is able to prepare a control module input with readily available engineering parameters and keywords. The control module then automatically performs any

necessary data processing (e.g., cross-section preparation), generates the input to the functional modules, initiates module execution in proper sequence, and performs any needed postprocessing of the analytic results. Use of SCALE is further simplified by incorporation of a host of validated data bases (e.g., material compositions, thermal properties, cross sections) that allow easy input (via keywords) and data accessibility.

Version 3 of the SCALE system was used for the TMI-2 analyses. Four of the major functional modules (NITAWL-S, XSDRNP-S, KENO V.a, and ORIGEN-S) and three of the control module sequences (CSASIX, CSAS25, and SAS2) were employed. A brief summary of the capabilities of each module and control sequence is provided below.

1. The NITAWL-S module<sup>3</sup> applies the Nordheim integral technique to perform neutron cross-section processing in the resonance energy range. This technique involves a fine-energy-group calculation of the slowing down flux across each resonance with subsequent flux weighting of the resonance cross sections. The major function of NITAWL-S is its conversion of cross-section libraries from a problem-independent to a problem-dependent form. However, NITAWL-S also assembles group-to-group transfer arrays from the elastic and inelastic scattering components and performs other tasks in producing the problem-dependent working library.

2. The KENO V.a module<sup>4</sup> is a multigroup Monte Carlo code employed to determine effective multiplication factors ( $k_{eff}$ ) for multidimensional systems. The basic geometrical bodies allowed for defining the model are cuboids, spheres, cylinders, hemispheres, and hemicylinders. KENO V.a differs from KENO IV in that it (a) has an enhanced geometry package that allows arrays to be defined and positioned throughout the model, (b) has a  $P_n$  scattering treatment, (c) allows extended use of differential albedo reflection, (d) can generate printer plots for checking the input model, (e) supergroups energy-dependent data, (f) has an improved restart capability, and (g) allows the origin location to be specified for spheres, cylinders, hemicylinders, and hemispheres.

3. The XSDRNP-S module<sup>5</sup> is a one-dimensional discrete ordinates transport code for performing neutron or coupled neutron-gamma calculations. The code has a variety of uses within SCALE: preparation of cell-averaged cross sections for subsequent system analysis, one-dimensional criticality safety and radiation shielding analysis, and generation of a neutron spectrum to develop spectral parameters for ORIGEN-S.

4. The ORIGEN-S module<sup>6</sup> is an updated version of the ORIGEN code<sup>7</sup> with flexible dimensioning and free-form input processing. One of the primary objectives in developing ORIGEN-S was that the calcula-

tions be able to utilize multi-energy-group neutron flux and cross sections in any group structure. Utilization of the multigroup data is automated via the COUPLE code. ORIGEN-S performs point depletion and decay analyses to obtain isotopic concentrations, decay heat source terms, and radiation source spectra and strengths for use in subsequent system analyses.

5. CSASIX and CSAS25 are sequences within the CSAS4 control module.<sup>8</sup> The primary product from CSASIX is resonance-corrected, cell-weighted mixed cross sections in a working library format. The automated computational sequence is NITAWL-S, XSDRNP-S, and ICE-S, which performs the cross-section mixing. The CSAS25 sequence uses NITAWL-S and KENO V.a in sequence to perform a Monte Carlo analysis to obtain the system  $k_{eff}$ .

6. The SAS2 sequence<sup>9</sup> employs the sequence of Fig. 1 to perform a depletion analysis and subsequent one-dimensional cask shielding analyses. For the TMI-2 efforts, the SAS2 sequence was halted following the final ORIGEN-S burnup and decay analysis that produced the spent-fuel isotopes. The ORIGEN-S spectral parameters and nuclear data library are updated by COUPLE using the flux spectrum and collapsed cross sections from an XSDRNP-S calculation for an infinite lattice representation of a fuel assembly.

The CSASIX, CSAS25, and SAS2 sequences all use the material information processor to read and process the composition and geometry information. For the XSDRNP-S cell analyses, each sequence utilizes a standard prescription for discrete ordinates quadrature type and order, scattering expansion order, spatial mesh specifications, and convergence criteria ( $10^{-4}$ ). For lattice cell geometries, input information on the lattice type (keyword selection), the lattice pitch, and the moderator total cross section is used to obtain the Dancoff factor using numerical integration routines from the SUPERDAN program.<sup>10</sup> Note that only one type of lattice cell can be specified in the input.

The CSASIX sequence was used exhaustively in the TMI-2 effort to analyze various combinations of lattice type, lattice pitch, fuel pellet diameter, and moderator. Many of the finite system models required problem-dependent cross sections from multiple CSASIX cases. The AWL module of the AMPX system<sup>11</sup> was used to combine the needed cross-section sets into one working library. Once the desired working library was available, the XSDRNP-S or KENO V.a module could be used in a stand-alone fashion to obtain  $k_{eff}$  for a finite system.

#### Cross-Section Data

The SCALE 27-group, ENDF/B-IV neutron cross-section library was applied for the TMI-2 analyses. This library was supplemented with ENDF/B-V data for fission product nuclides. This extension of the

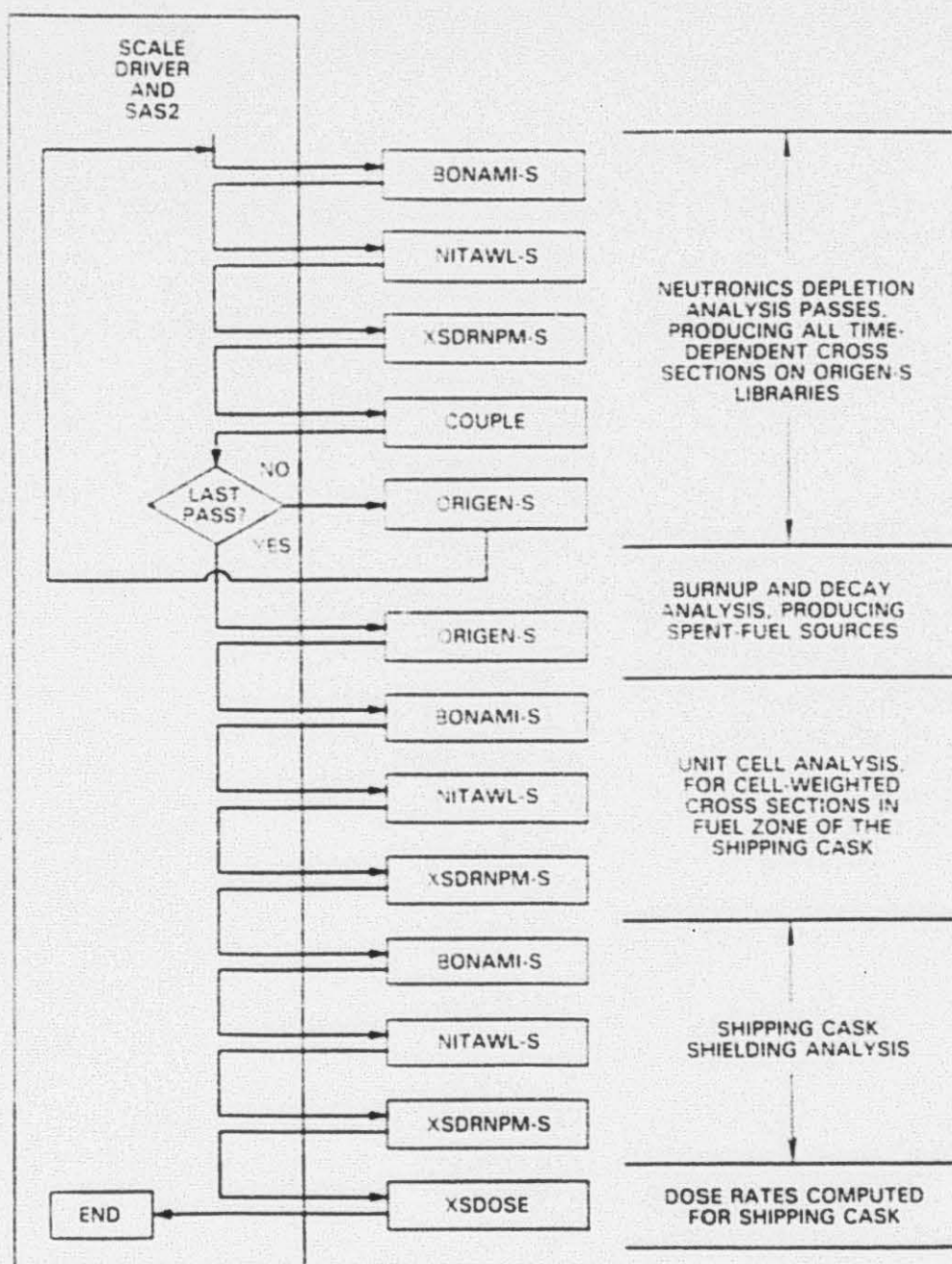


Fig. 1. Computational analysis scheme used by SAS2.

standard ENDF/B-IV library is necessary for depletion analyses and for criticality analyses where fission products are considered. The 27-group library has a  $P_3$  scattering expansion order and treats thermal upscatter to 3 eV. Validation of the library has been performed through calculation of critical experiments containing the fuel, structural materials, and neutron absorbers commonly found in cask and storage pool designs.<sup>12</sup>

A summary of the performance of the SCALE 27-group ENDF/B-IV library in the analysis of low-enriched, water-moderated systems is given in Table I. The systems are ordered, left to right, on the basis of increasing moderation. Two aspects of the experiments should be noted and discussed. The  $\text{UO}_2$  pin lattices were designed to simulate a  $3 \times 1$  array of fuel assemblies separated by water gaps and absorber plates. Also, the uranium metal pin lattice experiments were

TABLE I

Performance of the SCALE 27-Group ENDF B-IV Library on Low-Enriched, Water-Moderated Systems

Analytical reference	13	12	12	13	13
Number of experiments	25	35	35	14	10
Fuel enrichment and geometry	Uranium (4.89) metal pin lattice	U(4.29)O <sub>2</sub> pin lattice	U(2.35)O <sub>2</sub> pin lattice	Uranium (4.89) metal pin lattice	U(4.89)O <sub>2</sub> F <sub>2</sub> single units
Moderator	H <sub>2</sub> O	H <sub>2</sub> O	H <sub>2</sub> O	U(4.89)O <sub>2</sub> F <sub>2</sub> solution*	U(4.89)O <sub>2</sub> F <sub>2</sub> solution*
Fixed absorbers	None	Yes <sup>a</sup>	Yes <sup>b</sup>	None	None
Minimum $\bar{K}_{eff}$	0.985 ± 0.003	0.974 ± 0.004	0.986 ± 0.004	0.985 ± 0.003	0.991 ± 0.003
Maximum $\bar{K}_{eff}$	0.994 ± 0.003	0.997 ± 0.004	1.004 ± 0.004	1.006 ± 0.002	1.005 ± 0.002
Average $\bar{K}_{eff}$	0.989	0.988	0.994	0.995	0.997
H/ <sup>235</sup> U atom ratio, cell <sup>c</sup>	78 to 237	246	398	209 to 471	524 to 1099

Uranium at 300 g/t.

Type 304L stainless steel, stainless steel + boron, cadmium, Boral, copper, zirconium, aluminum.

Minimum bounding values assuming uniform lattices.

performed with various patterns of water gaps created by lattice vacancies. The fixed absorber plates, as well as the fluorine, are not considered to have a significant effect on the neutron energy spectrum. However, for any particular experiment, the additional water due to lattice vacancies will increase the H/<sup>235</sup>U atom ratio above the values shown in Table I.

Given these qualifications, the results for all 119 critical experiments support two general observations:

1. The average values for the calculated system multiplication factors vary from somewhat more than 1%  $\Delta k$  low for the dryer systems to approximately critical for the well-moderated systems.
2. The maximum deviation from the average value for any particular set of experiments is quantitatively on the order of the 3 standard deviation uncertainty associated with a 99.7% confidence level.

In summary, the results indicate a positive trend with neutron moderation, and their distribution is consistent with expected statistical behavior.

#### ANALYTICAL BIAS

The general performance of the 27-group ENDF/B-IV cross-section library for low-enriched, water-moderated systems was included above. To validate the lower vessel rubble study, a set of ten critical experiments was selected from an extensive list of candidates compiled by Murray<sup>14</sup> in consultation with staff members of the Babcock & Wilcox Company (B&W) and Bechtel. These experiments were chosen to emphasize the relatively hard neutron spectrum resulting from the high soluble boron level and low water content of the TMI-2 fuel rubble at optimum moderation. Characteristics of the selected experiments are shown in Table II.

along with the characteristics of the damaged and undamaged TMI-2 pin cell. The TMI-2 pin cell cases show how the boron, moderating ratio, and water-to-fuel ratio compared with the selected critical experiments.

The ten critical experiments were selected from the results of three experimental programs. In the B&W spectral shift<sup>15</sup> and Argonne National Laboratory (ANL) high-conversion<sup>16</sup> experiments, uniform pin lattices were subjected to soluble boron level or lattice-pitch variations to change the neutron spectrum. The B&W close-packed module experiments<sup>17</sup> simulate 25 fuel assemblies at various stages of compaction and are driven critical by neutron moderation due to the water gaps between the assemblies. The latter set of experiments also included a soluble boron variation.

Each of the experiments was analyzed with the 27-group ENDF/B-IV cross sections applied in KENO V.a. Four of the experiments (ANL-3, -11, -13, and B&W-2452) were modeled with homogeneous fuel regions with cell-averaged constants obtained with XSDRNPM-S. The results of the analyses are given in Table II.

The results for the uniform lattice experiments (B&W-10, -11, -12, -13, and ANL-3, -11, -13) are consistent with the earlier observations based on the summary of analyses in Table I. That is, this cross-section library yields critical values for well-moderated systems and a negative bias for low-moderated systems. The bias does not appear to be affected by the soluble boron level.

The results for the close-packed modules (B&W-2452, -2485, and -2500) do not show a consistent trend with either neutron moderation or soluble boron level. The presence of the borated water gaps between the modules could be a factor in the relatively poor analytical performance for these systems.

TABLE II  
Analysis of Critical Experiments for TMI-2 Benchmarking\*

Series	Case	Enrichment (wt%)	Boron (wppm)	Moderating Ratio*	Water/Fuel Volume Ratio	Multiplication Factor, $k_{eff}$
B&W spectral shift	10	4.02	0	2.17	1.14	$1.0062 \pm 0.0038$
	11	4.02	1152	2.02	1.14	$0.9961 \pm 0.0040$
	12	4.02	2342	1.88	1.14	$1.0087 \pm 0.0032$
	13	4.02	3389	1.77	1.14	$1.0088 \pm 0.0035$
ANL high conversion	3	3.042	0	3.33	1.37	$1.0008 \pm 0.0041$
	11	3.042	0	1.90	0.75	$1.0008 \pm 0.0039$
	13	3.042	0	1.13	0.43	$0.9861 \pm 0.0039$
B&W close-packed modules	2452	2.549	435	0.50	0.15	$0.9961 \pm 0.0038$
	2485	2.549	886	1.15	0.38	$0.9800 \pm 0.0018$
	2500	2.549	1156	2.67	1.01	$0.9942 \pm 0.0019$
TMI-2 pin cell	Undamaged	1.57	3500	2.98	1.65	0.9492
	Damaged	1.57	5000	1.49	0.72	0.9913

SCALE 27-group ENDF/B-IV library in KENO V; a second analysis of B&W-2485 was performed with the SCALE 123-group GAM-THERMOS library.

Table 2 of Ref. 14. This is the ratio of slowing down power to thermal absorption.

The results of this limited series of analyses support a 2.5%  $\Delta k$  analytical bias, taking the worst case and statistical uncertainty as a bounding value. This analytical bias was used throughout the TMI-2 defueling effort. Thus, since a  $k_{eff}$  criterion  $\leq 0.99$  was established for the RCS (Ref. 1), the 2.5%  $\Delta k$  bias limited the calculated  $k_{eff}$  value to a maximum of 0.965.

## DEPLETION ANALYSES

A schematic of the TMI-2 initial core loading is shown in Fig. 2. Depending on the physical system being analyzed, it was often desirable to use the isotopes consistent with the burned state of the fuel as opposed to the unrealistic, but conservative, fresh fuel isotopes. Thus, an SAS2 calculation was performed for each batch of fuel based on the reactor history and batch average exposure supplied by the Defueling Design Team.<sup>15</sup>

The analyses were run to burnups of 2745 MWd/tonne U for batch 1, 3051 MWd/tonne U for batch 2, and 2535 MWd/tonne U for batch 3. The batch 1 and 2 exposures are values for March 19, 1979. The batch 3 burnup of 2535 MWd/tonne U was obtained for the time of the accident (March 28) by scaling the March 19 value (2202 MWd/tonne U) on the basis of the average burnup for the two dates. Each of the SAS2 analyses used a simplified exposure history consisting of two fuel burns (45.2 and 49.4 days) and an interim

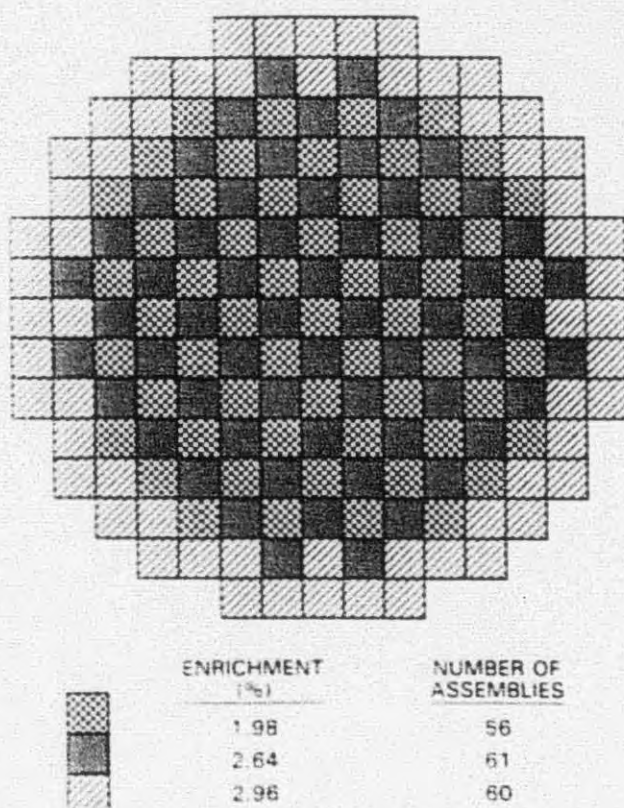


Fig. 2. TMI-2 initial core loading pattern.

downtime of 27 days. The specific power was 29.02 MW/tonne U for batch 1, 32.25 MW/tonne U for batch 2, and 26.5 MW/tonne U for batch 3. The isotopes were decayed 2075 days, consistent with a March 28, 1979–December 1, 1984, time interval.

The burnup analysis was performed for the fuel pin lattice according to the design specifications.<sup>12</sup> Operating conditions included an average fuel temperature of 1000 K, a water temperature of 579 K, and a water density of 0.7147 g/cm<sup>3</sup>. The soluble boron history for the TMI-2 reactor was obtained from the TMI-2 chemistry log book 1978, 1979 (Ref. No. CHEM-2-102). These data were weighted by the power history to obtain average values of 1330.3 weight parts per million (wppm) boron for the first burn period and 1093.9 wppm boron for the second burn period.

To alleviate concerns regarding the failure to account for the axial burnup variation, a brief study was performed to assess the effect of axial variation on

The results of the study<sup>13</sup> indicated that the axial effect was at most 0.2%  $\Delta k$  for systems of interest. The small magnitude of this effect coupled with the very low probability of the rubble being segregated by fuel burnup effectively counters the concern about ignoring the axial variation of the burnup.

#### SPHERICAL RUBBLE MODEL

In all of the finite system analyses, the fuel was represented as a homogeneous medium for which the cross-section data correspond to a triangular lattice of spherically shaped fuel pellets. A schematic of the rubble media is shown in Fig. 3. To maximize the reactivity worth of the fuel cross sections, the presence of fuel cladding, fixed absorbers, and structural materials was

ignored. To further maximize reactivity, the density of the UO<sub>2</sub> spheres was taken as the pellet design density of 10.3 g/cm<sup>3</sup>. A search was typically performed for each moderator change to determine the lattice pitch (and so the corresponding fuel volume fraction) that gave the maximum  $k_{\infty}$  value for the lattice of specified spherical pellets. For the vast majority of the analyses, the surface-to-mass ratio of the cylindrical design pellet was preserved in specifying the spherical pellet size (1.0724 cm). However, for some system analyses, the uncertainty in the actual rubble particle size required an optimization of  $k_{\infty}$  by searching both pellet size and lattice pitch.

Separate analyses were performed to gauge the conservatism provided by some of the above assumptions. The results indicate that in the range of 3500 to 4500 wppm soluble boron in water, the presence of zircaloy clad in the model would reduce the maximum lattice cell multiplication factor by ~2%  $\Delta k$ . Consideration of the heterogeneous UO<sub>2</sub> pellet/water mixture rather than a homogeneous UO<sub>2</sub>/water slurry increases the multiplication factor by 3%  $\Delta k$ . Note that a model based on an unclad fuel pin of infinite height and design diameter would be worth ~1%  $\Delta k$  more than the spherical pellet model applied in this study. However, the spherical pellet model corresponds to an optimum credible arrangement of the fuel pellets, considering a random fuel reassembly following core disruption.

The CSASIN module was used to obtain the neutronic constants from an infinite lattice cell analysis of the rubble model. CSASIN uses the SUPERDAN algorithms to obtain the Dancorff factor for the 12-sided, dodecahedral unit cell applied in the resonance shielding analysis performed by NITAWL-S.

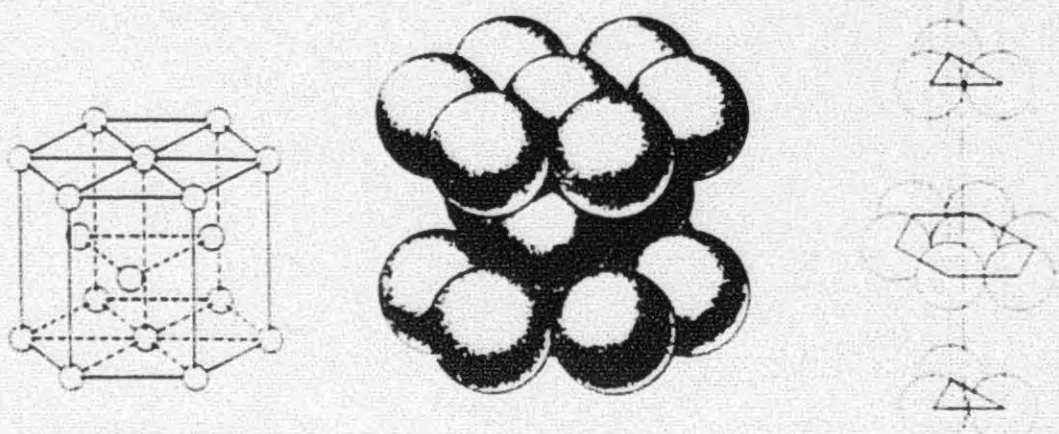


Fig. 3. Spherical rubble model.

The equivalence between this unit cell and the two-region, spherical unit cell applied in the subsequent XSDRNP-S cell-averaging calculation comes from the preservation of the fuel volume fraction (VF). As derived from Cundy and Rollett,<sup>23</sup> the fuel VF in the dodecahedral cell is given by

$$\text{Fuel VF} = \frac{4\sqrt{2}}{3} \pi (r/P)^3,$$

where

$r$  = fuel pellet radius

$P$  = lattice pitch.

Values for  $r$  and  $P$  are input to CSASIN, which then calculates the outer radius (i.e., moderator region) of the equivalent (identical VF) spherical unit cell.

For pin lattice geometries that can be represented explicitly in KENO V.a, comparisons have been made between the use of neutronic constants that have been cell-averaged in XSDRNP-S according to the above prescription and neutronic constants processed by NITAWL-S for the specific lattice. Thus, in both cases the end analysis was done with KENO V.a, one with cell-averaged constants, the other with the fuel lattice represented explicitly. The good agreement in the results indicates the effectiveness of the XSDRNP-S cell-averaging procedure. Note that the KENO V.a geometry package cannot represent the dodecahedral cell boundary explicitly, and thus the cell averaging of neutronic constants was a necessity for this rubble model.

### INFINITE LATTICE CELL ANALYSES

As implied above, hundreds of infinite lattice cell analyses were performed in order to provide a neutronic characterization of the rubble model and generate cell-averaged cross sections that produced the highest (optimum)  $k_{\infty}$  values. Optimum  $k_{\infty}$  searches were performed with CSASIN by varying the pitch (and so the VF) for the particular pellet and moderator condition. Table III provides a summary of results from the infinite lattice cell analyses. The table primarily reports the results for rubble conditions used in finite system analyses. However, many more analyses were needed to (a) determine the optimum fuel VF, (b) study the effect of temperature changes on  $k_{\infty}$ , (c) understand the relative effect of individual spent-fuel nuclides on  $k_{\infty}$ , and (d) characterize the variation in  $k_{\infty}$  for fuel particle sizes other than that corresponding to the design pellet.

For boron levels between 0 and 4950 wppm, searches for the optimum fuel VF were performed for  $^{235}\text{U}$  enrichments ranging from 2.11 (average enrichment of batches 1 and 2 after depletion) to 2.96 wt% (initial enrichment of batch 3). For batch 3 fuel, Table III provides an indication of the change in optimum VF as a function of soluble boron level. The

optimum fuel VF varies only slightly with enrichment. For unborated systems, the optimum VF becomes more sensitive to changes in enrichment. Typically, for highly borated systems, the optimum VF found for one enrichment was assumed to be sufficient for other enrichments in the noted range. Between 4350 and 4950 wppm boron, the optimum fuel VF varies from 0.61 to 0.68; at 0 wppm boron, the variation is 0.28 to 0.33. An initial study was performed to demonstrate that for high boron levels, there was a change of only  $-0.05\Delta k/10\text{ K}$  (Ref. 18). All subsequent analyses were performed at 293 K.

An initial study was also made to demonstrate the differential worth of including the major spent-fuel nuclides in the cell analyses. The isotopic results from the batch 3 burnup case were used. The analyses were done using design pellet particle sizes (1.0724-cm diam) and 4750 wppm soluble boron in water. The results of these analyses are summarized in Table IV. Twenty-nine actinide and fission product isotopes were included in the most comprehensive calculation, case 9. Based on these analyses, the overall batch 3 burnup has a potential worth of  $1.76\Delta k$ . For all subsequent analyses with spent-fuel isotopes, the nuclides of case 9 were employed. Note, however, that searches for optimum VF and/or particle size were performed with the non-uranium actinides and fission products removed in order to eliminate the need for resonance processing of these nuclides by NITAWL-S. This practice enabled a 66% reduction in central processing unit (CPU) time with essentially no effect on characterizing the optimum conditions.

As evidenced by Table III, the vast majority of lattice calculations was done assuming a spherical  $\text{UO}_2$  diameter (1.0724 cm) corresponding to the design pellet size. However, larger particle diameters were assumed if  $\text{UO}_2$  melting and resolidification were postulated. Thus, during the support effort, several searches on both particle size and VF were performed for specified fuel types and soluble boron levels. For high boron levels (4950 wppm), the optimum particle diameter was 3.5 to 3.8 cm. This diameter decreased to  $\sim 2.1$  cm for the unborated case. Table V provides an example of the variation in  $k_{\infty}$  as the particle diameter changes. The scenario of melting and resolidification also implies that other material in the core would be mixed with the resolidified particle. Samples taken from the lower head debris showed impurity materials, as listed in Table VI. An infinite cell analysis using optimum particle size and VF for this mixture yields a  $k_{\infty}$  of only 0.7600.

A study of very small particle sizes was also initiated to ensure that a conservative approach was being used for situations where small debris were known or postulated to be present. The small particle situations of interest to the TMI-2 Defueling Design Team involved an unborated water moderator. This condition, in combination with small particle sizes ( $<0.4\text{-cm}$

TABLE III  
Fuel Rubble Lattice Cell Analyses

Material Code	Fuel Description <sup>a</sup>	Enrichment (wt% $^{235}\text{U}$ )	Fuel Particle Diameter <sup>b</sup> (cm)	Fuel VF	Soluble Boron (wppm)	Infinite Multiplication Factor, $k_{\infty}$
A	Fresh batch 3	2.96	1.0724	0.63 <sup>c</sup>	4750	0.9923
B	Fresh batch 3	2.96	1.0724	0.61 <sup>c</sup>	4200	1.0111
---	Fresh batch 3	2.96	1.0724	0.57 <sup>c</sup>	3500	1.0386
---	Fresh batch 3	2.96	1.0724	0.53 <sup>c</sup>	2500	1.0925
---	Fresh batch 3	2.96	1.0724	0.50 <sup>c</sup>	2000	1.1260
---	Fresh batch 3	2.96	1.0724	0.42 <sup>c</sup>	1000	1.2197
---	Fresh batch 3	2.96	1.0724	0.35 <sup>c</sup>	500	1.2911
C	Fresh batch 3	2.96	1.0724	0.28 <sup>c</sup>	0	1.4009
---	Fresh batch 3 in HF <sup>d</sup>	2.96	1.0724	0.265 <sup>c</sup>	0	1.4020
D	Fresh batches 1 and 2	2.54	1.0724	0.63	4950	0.9199
E	Fresh batches 1 and 2	2.54	1.0724	0.66 <sup>c</sup>	4950	0.9211
F	Fresh batches 1 and 2	2.54	1.0724	0.63	4750	0.9254
G	Fresh batches 1 and 2	2.54	1.0724	0.61	4350	0.9382
H	Fresh batches 1 and 2	2.54	1.0724	0.61	4200	0.9439
I	Fresh batches 1 and 2	2.54	1.0724	0.30 <sup>c</sup>	0	1.3349
---	Fresh batches 1, 2, and 3	2.57 <sup>e</sup>	3.60 <sup>c</sup>	0.68 <sup>c</sup>	4950	0.9682
J	Fresh batches 1, 2, and 3	2.57 <sup>e</sup>	3.50 <sup>c</sup>	0.66 <sup>c</sup>	4350	0.9882
---	Fresh batches 1, 2, and 3	2.57 <sup>e</sup>	2.10 <sup>c</sup>	0.33 <sup>c</sup>	0	1.3724
K	Fresh batches 1, 2, and 3 (approximate)	2.50	1.0724	0.28 <sup>c</sup>	0	1.3540
L	Burned batch 3	2.67	1.0724	0.63 <sup>c</sup>	4950	0.9690
M	Burned batch 3	2.67	1.0724	0.63 <sup>c</sup>	4750	0.9747
N	Burned batch 3	2.67	1.0724	0.61 <sup>c</sup>	4350	0.9881
O	Burned batch 3	2.67	1.0724	0.61 <sup>c</sup>	4200	0.9929
P	Burned batch 3	2.67	1.0724	0.57 <sup>c</sup>	3500	---
Q	Burned batch 3	2.67	1.0724	0.53 <sup>c</sup>	2500	---
R	Burned batch 3	2.67	1.0724	0.50 <sup>c</sup>	2000	---
S	Burned batch 3	2.67	1.0724	0.42 <sup>c</sup>	1000	---
T	Burned batch 3	2.67	1.0724	0.35 <sup>c</sup>	500	---
U	Burned batch 3	2.67	2.8 <sup>c</sup>	0.55 <sup>c</sup>	2000	1.1194
V	Burned batch 3	2.67	1.0724	0.28 <sup>c</sup>	0	1.3667
W	Burned batch 3	2.67	2.1 <sup>c</sup>	0.33 <sup>c</sup>	0	1.3748
X	Burned batch 3	2.67	1.0724	0.63	0	1.1429
Y	Burned batch 3 in HF	2.67	1.0724	0.265 <sup>c</sup>	0	1.3680
Z	Burned batch 3 with impurities	2.67	3.0 <sup>c</sup>	0.40 <sup>c</sup>	0	0.7600
AA	Burned batches 1 and 2	2.11 <sup>f</sup>	3.5 <sup>c</sup>	0.66 <sup>c</sup>	4350	0.9594
BB	Burned batches 1, 2, and 3	2.32 <sup>f</sup>	3.6 <sup>c</sup>	0.68 <sup>c</sup>	4950	0.9595
CC	Burned batches 1, 2, and 3	2.32	3.5 <sup>c</sup>	0.66 <sup>c</sup>	4350	0.9784
DD	Burned batches 1, 2, and 3	2.32	2.10 <sup>c</sup>	0.33 <sup>c</sup>	0	1.3450
EE	Burned batches 1, 2, and 3	2.24 <sup>g</sup>	1.0724	0.28 <sup>c</sup>	0	1.3254
FF	Burned batches 1, 2, and 3	2.24	1.0724	0.66	4950	0.9287
GG	Burned batches 1, 2, and 3	2.24	3.8 <sup>c</sup>	0.69 <sup>c</sup>	5100	0.9448
HH	Burned batches 1, 2, and 3	2.24	3.6 <sup>c</sup>	0.68 <sup>c</sup>	4950	0.9496

<sup>a</sup>Spherical  $\text{UO}_2$  particles in full-density water except as noted. Burned fuel compositions contain fission products and plutonium.

<sup>b</sup>Design pellet corresponds to spherical particle of 1.0724 cm.

<sup>c</sup>Particle size and/or VF that yields the highest  $k_{\infty}$  value.

<sup>d</sup>HF = hydraulic fluid moderator, UCON WS-34; density = 1.029 g/cm<sup>3</sup>, molecular weight = 788 g/mol, stoichiometric ratio carbon/hydrogen/oxygen = 39/80/15.

<sup>e</sup>Average core enrichment is actually 2.54 wt%. This higher value obtained and used prior to obtaining correct information of Fig. 2.

<sup>f</sup>This average enrichment (and other burned isotopes) was obtained from conservative scaling of batch 3 depletion results prior to depletion analyses of batches 1 and 2.

<sup>g</sup>Enrichment and burned isotopes were obtained from separate depletion analyses of all batches of fuel.

TABLE IV  
 $k_{\infty}$  of Lattice of Batch 3 Rubble\* with Burnup

Case	Burnup Products (included in calculation)	$k_{\infty}$
1	Depleted $^{235}\text{U}$ , at 2.67 wt%	0.9633
2	Depleted $^{235}\text{U}$ + samarium	0.9531
3	Depleted $^{235}\text{U}$ , samarium and lanthanum	0.9530
4	Depleted $^{235}\text{U}$ , samarium, lanthanum, and cerium	0.9530
5	Depleted $^{235}\text{U}$ , samarium, lanthanum, cerium, and europium	0.9527
6	Depleted $^{235}\text{U}$ and 50% of samarium, lanthanum, cerium, and europium	0.9579
7	Plutonium isotopes only (with fresh fuel)	1.0100
8	Depleted $^{235}\text{U}$ , plutonium, samarium, lanthanum, cerium, and europium	0.9768
9	Depleted $^{235}\text{U}$ , plutonium, samarium, lanthanum, cerium, europium, promethium, neodymium, and praseodymium	0.9747*

\*Design pellet particle size in water with 4750 wppm soluble boron.

For fresh fuel assay (2.96 wt%) and no fission product,  $k_{\infty} = 0.9923$  and %  $\Delta k_{\infty} = 0.9923 - 0.9747 = 1.76\%$ .

TABLE V  
 Variation in  $k_{\infty}$  Versus Particle Size\*

Sphere Diameter (cm)	Optimum Fuel VF	$^{235}\text{U}(2.96)\text{O}_2$	$^{235}\text{U}(2.34)\text{O}_2$
0.724	0.61	1.0064	0.9382
1.4	0.61	1.0132	0.9462
1.6	0.62	1.0168	0.9494
2.2	0.65	1.0234	0.9571
2.5	0.66	1.0265*	
2.8	0.67	1.0246	0.9611
3.6	0.69	1.0144	0.9513
4.8	0.74*	1.0024	0.9427

$^{235}\text{UO}_2$  spherical particles in water with 4350 wppm boron. Sphere diameter and VF selected by interpolation of results at 2.2- and 4.4-cm particle sizes.

\*Spheres touching; maximum packing fraction.

TABLE VI  
 Fuel Particle Composition for Investigating Effect of Impurities in Resolidified Rubble

Constituent	wt%
$^{235}\text{U}(2.67)\text{O}_2$ (burned)	83.79
Zirconium	12.70
Iron	2.44
Chromium	0.75
Molybdenum	0.15
Boron	0.11
Manganese	0.06

diam) caused the Dancoff factor algorithms used in SCALE-3 to be inadequate because they considered only through third-nearest neighbors in spherical lattices.<sup>21</sup> For small-particle, low-absorption systems, outer neighbors are very important to an accurate evaluation of  $k_{\infty}$ . Thus, the Dancoff treatment for SCALE-3 was modified and compared against an explicit point cross-section treatment and lattice model as applied by the MCNP Monte Carlo code.<sup>21,22</sup> The  $k_{\infty}$  results for the comparison are shown in Table VII and indicate a decrease in  $k_{\infty}$  as the particle size decreases. The modified Dancoff treatment has been applied to Version 4 of the SCALE system and has been utilized in subsequent analyses where small particles had to be considered.

## APPLICATIONS AND RESULTS

### Lower Vessel Rubble Studies

After selecting the dodecahedral unit cell as the rubble model, the first application effort was to establish a concentration of soluble boron that would maintain the core in a shutdown configuration for all fuel removal operations. Several simple models were developed and analyzed for this task.

Each of the models applied in the lower vessel study included fuel/rubble and borated water regions contained in a 20.32-cm (8-in.)-thick Type 304 stainless steel reflector representative of the hemispherically

\*The Dancoff correction factor is the first-flight transmission probability through the interstitial material between fuel lumps. It is applied by NITAWL-S to the leakage from the single lump in order to approximate the effects of a lattice of fuel lumps.

TABLE VII  
Comparison of  $k_{\infty}$  Values for Lattice of Dodecahedral Cells\*

Fuel VF	Spherical Particle Diameter (cm)	Infinite Multiplication Factor, $k_{\infty}$		
		SCALE-3	Modified SCALE (SCALE-4)	MCNP
0.33	1.0	1.326	1.328	$1.321 \pm 0.002$
0.33	0.6	1.302	1.309	
0.33	0.5	1.291	1.302	
0.33	0.4	1.277	1.295	$1.292 \pm 0.003$
0.33	0.3	1.256	1.287	
0.33	0.2	1.220	1.277	
0.33	0.02	0.881 <sup>a</sup>	1.260 <sup>a</sup>	$1.249 \pm 0.010$
0.33	0.002	0.570 <sup>a</sup>	1.265 <sup>a</sup>	
0.33	Infinite homogeneous	1.254	1.254	$1.251 \pm 0.002$
0.63	1.0	1.131	1.133	$1.139 \pm 0.003$
0.63	0.6	1.105	1.112	
0.63	0.5	1.094	1.106	
0.63	0.4	1.081	1.100	$1.105 \pm 0.005$
0.63	0.3	1.062	1.093	
0.63	0.2	1.031	1.085	$1.102 \pm 0.006$
0.63	Infinite homogeneous	1.093	1.093	$1.082 \pm 0.002$

\*Spherical U(2,32)O<sub>2</sub> particle in unborated water.

<sup>a</sup>The NSDRNPM cases did not converge in 25 outer iterations.

shaped lower portion of the pressure vessel. The presence of steel members interior to the vessel (such as the lower grid and the flow distributor) was ignored as a conservative approximation.

The models characterized the fuel region as having one of three geometry shapes: spherical, lenticular or lens-shaped, and semilenticular or flattop. The first two models are shown in Figs. 4 and 5. Dimensions for the various zones are determined based on the inventory information supplied by the Defueling Design Team and the specified (or optimum) VF. For the lenticular model, the outer spherical shell of Type 304 stainless steel was always specified to have an outer dimension of 237.998 cm, which was the actual radius of curvature for the pressure vessel. The volume of a lenticular region is given by

$$V = 2\pi h^2(r - h/3),$$

where

$h$  = region's half-height

$r$  = radius of curvature of the outer lenticular surface.

The fuel volume of the flattop model is one-half of this value. For a given fuel volume, leakage considerations

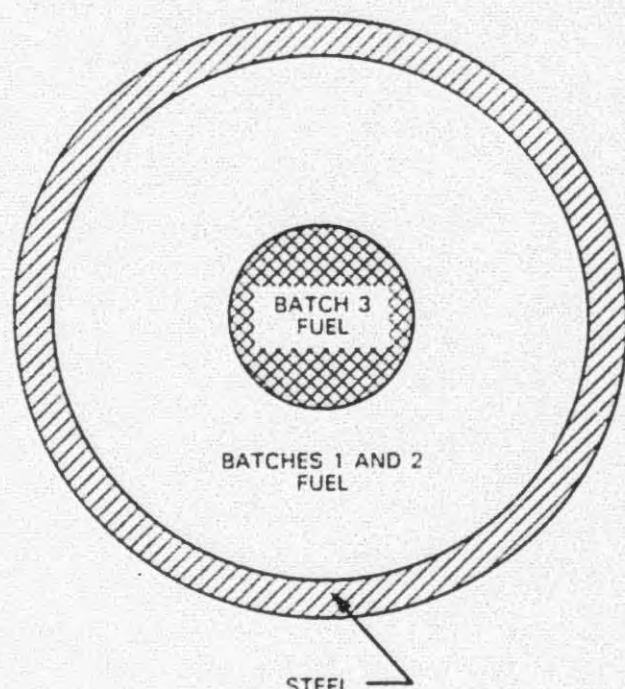


Fig. 4. Multizone spherical model.

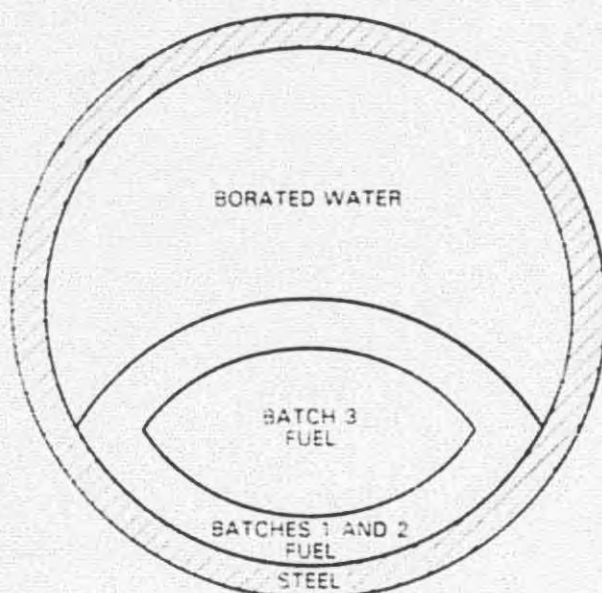


Fig. 5. Lenticular fuel model.

from elementary reactor theory predict that the spherical fuel geometry is the most reactive. The lenticular and flattop fuel geometries produce progressively more leakage and are therefore less reactive. Thus, the idealized spherical fuel geometry is the most conservative from the criticality safety standpoint, while the other models are less conservative but more realistic. Also, note that the spherical model is amenable to highly precise analysis with the one-dimensional discrete ordinates code, XSDRNPM-S.

The primary results for the finite system analyses are listed in Table VIII. The lenticular model was selected as the design-basis model because it provided the best combination of realism, simplicity, and conservatism. Case 1 is the design-basis case, showing that a soluble boron level of 4350 wppm is just under the calculational limit of 0.965. The fuel arrangement for the base case and most other cases of Table VIII was conservative but somewhat unrealistic since batch 3 fuel was placed as the central fuel zone. Comparisons of cases 4 and 5, 6 and 8, and 7 and 9 indicate that the use of burned batch 3 isotopes provides a reactivity decrease of 1.6 to 1.8%  $\Delta k$  in comparison with fresh batch 3 isotopes. This finding is consistent with the results shown in Table IV for an infinite lattice.

Although not used as the design basis, the spherical model proved to be very valuable for scoping and parameter studies. To be utilized effectively, it was necessary to define the differential reactivity worth between the hypothetical spherical model and the more plausible lenticular model. Comparisons of case 1 and 2, 3 and 4, 6 and 7, and 8 and 9 of Table VIII — a

0.3%  $\Delta k$  decrease in reactivity in going from the spherical to lenticular model. In addition, cases 7 and 9 were analyzed with XSDRNPM-S and KENO V.a to confirm that the two codes yielded identical results within the statistics provided by the Monte Carlo analysis.

The boron worth is another variable that can be characterized by the results of Table VIII. Comparison of cases 4 and 7 shows a 1.83%  $\Delta k$  increase in reactivity in going from 4750 to 4200 wppm boron. Cases 5 and 9 show an effect of 1.68%  $\Delta k$ . These values predict a boron reactivity worth of -300 to 330 wppm/1%  $\Delta k$ . The infinite lattice data in Table III predict a boron worth in agreement with these values. Also, on the basis of a unit of boron concentration, the data demonstrate a decreasing boron worth with increasing boron level.

New observations made subsequent to the design-basis study revealed large chunks of apparently once-molten and resolidified UO<sub>2</sub> present in the TMI-2 lower vessel. A study was then undertaken to determine if a larger, reconfigured pellet might be more reactive than the particle size consistent with the design fuel pellet. Finite system models were defined to demonstrate the reactivity effects of various modifications to the defueling design-basis case. The major features of these modifications were based on early (circa 1985) core damage assessments that included an estimated 20 to 30% core melt with a high likelihood of the molten fuel being from batches 1 and 2. The approach taken in modifying the design-basis case was to introduce the optimum-particle-size fuel into the central, most reactive zone of the models.

Cases 10 through 14 of Table VIII show the results of the analysis performed with optimum-particle-size fuel using the spherical core model (to better obtain accurate reactivity differences). Comparisons of cases 1 and 10 indicate a 0.19%  $\Delta k$  increase using the new model of case 10. Progressively adding burnup and going from 20 to 30% of the inventory (cases 10 to 12) shows a sequential decrease in the multiplication factor. The model of case 13 incorporates the likelihood that all of the molten fuel was from batches 1 and 2. The model of case 14 has the batch 3 fuel on the core periphery, corresponding to its actual location in the reactor core. Both cases show substantial decreases in  $k_{eff}$ .

The overall conclusion of the study with optimum particle size is that while a larger particle size is more reactive than the design pellet, incorporation of the larger particle into finite systems that are consistent with the core damage assessment leads to a reduction in the system multiplication factor.

#### Limits of Foreign Materials

Once the design-basis model and limiting soluble boron level were determined and approved, defueling operations were able to begin at TMI-2. The first

TABLE VIII  
Results of TMI-2 Lower Vessel Rubble Studies

Case	Model Description	Material Code Sequence <sup>a</sup> [outer radius or half-height, radius of curvature (cm)]	Soluble Boron Level (wppm)	Analysis Code	Multiplication Factor, $k_{eff}^b$
1	Fig. 5, design-basis case	N(81,414,151,777) G(116,754,217,678) Type 304 stainless steel (237.998)	4350	KENO V.a	$0.9646 \pm 0.0017$
2	Fig. 4, spherical equivalent of design-basis case	N(107,41) G(154,04) Type 304 stainless steel (174.36)	4350	XSDRNPMS	0.9671
3	Fig. 5, case 1 at lower boron	O(81,414,151,777) H(116,754,217,678) Type 304 stainless steel (237.998)	4200	KENO V.a	$0.9688 \pm 0.0016$
4	Fig. 4, spherical equivalent of case 3	O(107,41) H(154,04) Type 304 stainless steel (174.36)	4200	XSDRNPMS	0.9720
5	Fig. 4, case 4 with fresh batch 3 fuel	B(107,41) H(154,04) Type 304 stainless steel (174.36)	4200	XSDRNPMS	0.9884
6	Fig. 5, case 1 at higher boron	M(79,9565,151,777) F(114,673,217,678) Type 304 stainless steel (237.998)	4750	KENO V.a	$0.9520 \pm 0.0018$
7	Fig. 4, spherical equivalent of case 6	M(106,26) F(152,40) Type 304 stainless steel (172.72)	4750	XSDRNPMS KENO V.a	0.9537 $0.9548 \pm 0.0016$
8	Fig. 5, case 6 with fresh batch 3 fuel	A(79,9565,151,777) F(114,673,217,678) Type 304 stainless steel (237.998)	4750	KENO V.a	$0.9685 \pm 0.0020$
9	Fig. 4, spherical equivalent of case 8	A(106,26) F(152,40) Type 304 stainless steel (172.72)	4750	XSDRNPMS KENO V.a	0.9716 $0.9723 \pm 0.0014$
10	4-zone sphere, 20% core melt, fresh	J(87.75), N(118.60) G(153.28) Type 304 stainless steel (173.60)	4350	XSDRNPMS	0.9690
11	4-zone sphere, 20% core melt, burned	CC(87.75), N(118.60) G(153.78) Type 304 stainless steel (173.60)	4350	XSDRNPMS	0.9624
12	Case 11, 30% core melt	CC(100.45), N(123.44) G(152.88) Type 304 stainless steel (173.20)	4350	XSDRNPMS	0.9618
13	4-zone sphere, 20% 1 and 2 melt, burned	AA(76.44), N(119.02) G(153.53) Type 304 stainless steel (173.85)	4350	XSDRNPMS	0.9576
14	4-zone sphere, 20% 1 and 2 melt, burned, 3 outside	AA(76.44), G(133.51) N(153.53) Type 304 stainless steel (173.85)	4350	XSDRNPMS	0.9385

<sup>a</sup>See Table III for fuel material codes.

<sup>b</sup>Four decimal places are given for comparison. The basic precision is only one figure in the third decimal place or 0.1%  $\Delta k$ .

criticality concern to arise was the effect that various foreign materials would have if intentionally or accidentally inserted into the RCS. The lower operational limit on soluble boron (4950 wppm) was used to establish the limiting reactivity worth of foreign materials. Case 1 of Table IX shows the spherical equivalent of the design-basis case for the 4950 wppm boron level. A comparison with case 2 of Table VIII indicates a 1.93%  $\Delta k$  margin is available in moving the design-basis case from 4350 to 4950 wppm. Thus, a limiting calculated  $k_{eff}$  value for the foreign material spherical models was set equal to the  $k_{eff}$  value for the spherical equivalent design-basis case at 4950 wppm boron plus a 1.9%  $\Delta k$  reactivity margin (i.e.,  $0.9478 + 0.019 = 0.9668$ ). However, some spherical models utilized for this task differed from the design-basis fuel arrangement in that batch 1 and 2 fuel were placed in the center (cases 9, 10, and 16 through 19 of Table IX). Since these models were significantly different from the design-basis fuel arrangement, they were restricted to the calculational limit of  $k_{eff} < 0.965$ .

Several spherical foreign material models were developed to establish the limits of the materials as reflectors or interstitial moderators. Cases 2 through 10 of Table IX indicate the effect of various reflector materials between the fuel and the stainless steel shell. A maximum reflector thickness of 65 cm was considered. Beryllium (case 6) is the best reflector, with a 0.2%  $\Delta k$  increase over the base case. However, none of the reflectors, including the specularly reflecting boundary condition (case 8), exceeded the specified limit.

Cases 11 through 19 of Table IX summarize the interstitial moderator analyses. Each case represents a series of analyses to determine the limiting quantity of moderator for that particular model. As one would expect, the moderator is most effective when placed in the center of the model. Rather than a limiting quantity, the water thickness for case 14 yields the maximum multiplication factor calculated for a model with the water separating the batch 3 fuel. Thus, there is no limiting quantity of water for this configuration.

Cases 11 and 12 of Table IX indicate the limiting amount of fresh water and hydraulic fluid. In the analyses, these unborated moderator quantities were conservatively assumed to totally displace the borated coolant in the most reactive portion of the core model (center). Note also that optimum fuel VFs were used for each fuel zone. Case 13 indicates that using the optimum VF for the borated fuel in all fuel zones (including the zone with unborated water) provides a reactivity decrease of 1.4%  $\Delta k$ . Cases 16 through 19 were performed to ensure that the design-basis fuel arrangement (batch 3 centered) provided the most conservative limits on unborated water insertion.

As a result of the analyses presented in Table IX, the Defueling Design Team established the limits on foreign materials allowed to be introduced into the core. Note that there was extremely slow outer iteration convergence in the XSDRNPM-S calculations for the large spherical models of Table IX. In particular, the models with unborated central regions took >85 outer iterations<sup>7</sup> to reach a convergence criteria of 10<sup>-7</sup>. The slow convergence is due in large part to the large change in the spectrum between the unborated and highly borated regions. In many cases, when the convergence criteria was met,  $k_{eff}$  was still rising at a rate only slightly less than 10<sup>-4</sup> per outer iteration. Thus, estimates of an asymptotic  $k_{eff}$  were computed by extrapolating an assumed exponential error decay from the converged values. For the cases with unborated central regions, this practice typically produced an increase of 0.1%  $\Delta k$  over the "converged"  $k_{eff}$ .

**Safety Assessment for Use of a Plasma Arc Torch**

As part of the effort to dismantle the lower core support assembly (LCSA), it was necessary to utilize a plasma arc torch. To provide adequate cooling, the torch system needs ~15 l (4 gal) of H<sub>2</sub>O. Highly borated water could not be employed as a coolant because of its high electrical conductivity. Also, the limit on unborated water allowed in the core was set at 7.57 l (2 gal) based on the result from case 11 of Table IX. Thus, an effort was begun to generate a simple, yet conservative, model of the LCSA that would specifically address utilization of the plasma torch. The goal was to provide an acceptable model that would undergo a thorough criticality safety review and still allow the limit on unborated water to be raised.

As one might expect, this task entailed a considerable amount of back and forth iteration between the analysts, Defueling Design Team, operations personnel, and internal criticality safety reviewers. Table X shows the results that were performed initially to determine what boron level was needed to raise the underborated moderator limit to 15 l per the model of case 11 in Table IX. The table results indicate the torch cooling water would need 1000 wppm soluble boron to meet the  $k_{eff}$  criterion. However, the operations personnel then determined that any boron level was unacceptable for adequate torch operation. Thus, the Defueling Design Team began a thorough look at the LCSA geometry, information (available from the defueling activities) on the fuel characteristics in the LCSA, and scenarios for inserting the cooling water into fuel areas. The results of these analyses are shown in Table XI.

Case 1 of Table XI is the spherical base case LCSA model consisting of two fuel zones. The inner zone is burned batch 3 fuel in unborated water with optimum particle size and fuel VF. A study of the plasma torch

<sup>7</sup>The CPU time associated with these large numbers of outer iterations was reduced by 72% if a converged result was obtained via the XSDRNPM diffusion theory option prior to switching to the transport theory option.

TABLE IX  
Results of Foreign Material Study with Finite Spherical Systems

Case	Model Description	Number of Zones	Material Code Sequence <sup>a</sup> [Outer Radius (cm)]	Multiplication Factor <sup>b</sup>
1	Design basis, 4950 wppm boron, spherical equivalent	3	L(106.26), D(152.4) Type 304 stainless steel (172.72)	0.9478
2	Lead reflection	4	L(106.26), D(152.4), Lead (217.4) Type 304 stainless steel (237.72)	0.9481
3	Iron reflection	4	L(106.26), D(152.4), Iron (217.4) Type 304 stainless steel (237.72)	0.9493
4	Carbon reflection	4	L(106.26), D(152.4), Carbon (217.4) Type 304 stainless steel (237.72)	0.9493
5	Unborated water reflection	4	L(106.26), D(152.4), H <sub>2</sub> O(217.4) Type 304 stainless steel (237.72)	0.9486
6	Beryllium reflection	4	L(106.26), D(152.4) Beryllium (217.4) Type 304 stainless steel (237.72)	0.9496
7	Polyethylene reflection	4	L(106.26), D(152.4), C <sub>2</sub> H <sub>6</sub> (217.4) Type 304 stainless steel (237.72)	0.9486
8	Perfect reflection (outer boundary of core)	2	L(106.26), D(152.4)	0.9487
9	Base case with batches 1 and 2 (0.63 fuel VF) centered	3	D(132.76), L(152.4) Type 304 stainless steel (172.72)	0.9078
10	Beryllium reflection, batches 1 and 2 centered	4	D(132.76), L(152.4) Beryllium (217.4) Type 304 stainless steel (237.72)	0.9326
11	8.82 $\ell$ of unborated water (0.28 fuel VF) centered in batch 3	4	V(14.3), L(106.31), D(152.42) Type 304 stainless steel (172.74)	0.9657
12	9.19 $\ell$ of unborated hydraulic fluid centered in batch 3	4	V(14.4), L(106.31), D(152.42) Type 304 stainless steel (172.74)	0.9655
13	9.39 $\ell$ of unborated water (0.63 fuel VF) centered in batch 3	4	X(18.23), L(106.26), D(152.4) Type 304 stainless steel (172.72)	0.9519
14	2.5 cm of unborated water (no fuel) within batch 3	5	L(53.13), H <sub>2</sub> O(55.63) L(106.91), D(152.72) Type 304 stainless steel (173.04)	0.9637
15	486.92 $\ell$ of beryllium within batch 3	5	L(53.13), Beryllium (64.33) L(109.59), D(154.05) Type 304 stainless steel (174.37)	0.9668
16	Batches 1 and 2 centered, 1604 $\ell$ of unborated water in outer edge of batch 3	4	D(132.76), L(148.93), V(156.53) Type 304 stainless steel (176.85)	0.9634
17	Base case with batches 1 and 2 (0.66 fuel VF) centered	3	E(130.72), L(150.86) Type 304 stainless steel (171.18)	0.9090
18	1 and 2 (0.66 fuel VF) centered, 1576 $\ell$ of unborated water in outer edge of batch 3	4	E(130.72), L(147.39), V(154.99) Type 304 stainless steel (175.31)	0.9647
19	15.18 $\ell$ of unborated water (0.30 fuel VF) centered in batches 1 and 2 (0.66 fuel VF)	4	I(17.3), D(130.77), L(150.90) Type 304 stainless steel (171.22)	0.9636

<sup>a</sup>See Table III for fuel material codes.

<sup>b</sup>Four decimal places are given for comparison. The basic precision is only one figure in the third decimal place or 0.1% of  $k_{eff}$ .

TABLE X  
Results for 18,925  $\ell$  (4 gal) of Water with Varying Levels of Boron in Spherical Design-Basis Model

Case	Soluble Boron Level (wppm)	Material Code Sequence <sup>a</sup>	Multiplication Factor, $k_{eff}$
1	3500	P, L, D, Type 304 stainless steel	0.9496
2	2500	Q, L, D, Type 304 stainless steel	0.9519
3	2000	R, L, D, Type 304 stainless steel	0.9540
4	1000	S, L, D, Type 304 stainless steel	0.9653
5	500	T, L, D, Type 304 stainless steel	0.9823

<sup>a</sup>See Table III for fuel material codes.

<sup>b</sup>Four decimal places are given for comparison. The basic precision is only one figure in the third decimal place or 0.1%  $\Delta k_{eff}$ .

TABLE XI  
Spherical Model Results for Criticality Assessment of Using a Plasma Arc Torch to Cut the LCSA

Case	Model Description	Material Code Sequence <sup>a</sup> Outer Radius (cm)	Multiplication Factor, $k_{eff}$	
			NSDRNPM-S <sup>b</sup>	KENO V.a <sup>c</sup>
1	Base case LCSA model (11.355 $\ell$ unborated water)	W(15.935), FF(150.08) $H_2O$ with 4950 wppm boron (180.08)	0.9582	$0.9599 \pm 0.0013^d$
2	15.14 $\ell$ unborated water in core-average fuel optimum size	DD(17.538), BB(148.60)	0.9879	---
3	9.084 $\ell$ unborated water in 3 burned, optimum	W(14.793), BB(148.794) $H_2O$ with 4950 wppm boron (178.794)	---	$0.969 \pm 0.001$
4	9.841 $\ell$ unborated water in 3 burned, optimum	W(15.193), BB(148.597) $H_2O$ with 4950 wppm boron (178.597)	---	$0.966 \pm 0.001$
5	11.355 $\ell$ unborated water in 3 burned, optimum	W(15.935), BB(148.60) $H_2O$ with 4950 wppm boron (178.60)	---	$0.973 \pm 0.001$
6	9.841 $\ell$ unborated water in 3 burned	V(14.833), BB(150.797) $H_2O$ with 4950 wppm boron (180.797)	---	$0.967 \pm 0.001$
7	Base case with optimum particles in outer	W(15.935), HH(148.60) $H_2O$ with 4950 wppm boron (178.60)	0.9695	$0.9712 \pm 0.0011$
8	Case 7 with 5100 wppm boron in outer	W(15.935), GG(147.88) $H_2O$ with 5100 wppm boron (177.88)	0.9674	$0.9665 \pm 0.0013$
9	Mixing model	W(6.96), U(21.25), FF(150.08) $H_2O$ with 4950 wppm boron (180.08)	---	$0.924 \pm 0.001$

<sup>a</sup>See Table III for fuel material codes.

<sup>b</sup>Four decimal places are given for comparison. The basic precision is only one figure in the third decimal place or 0.1% of  $k_{eff}$ .

<sup>c</sup>All KENO V.a cases were run with 200 000 histories and a central start box extending 10 cm into region 2. Cases 3 through 6 and case 9 were run with 500 particles per generation and 400 generations; cases 1, 7, and 8 were run with 1000 particles per generation and 200 generations.

<sup>d</sup>This value is the mean and respective standard deviation obtained from ten separate KENO V.a cases (200 000 histories per case) where only the random number was changed.

as it would operate in the vessel found that it was hydraulically impossible to have more than 11.355  $\ell$  (3 gal) of water drain from the 15.14- $\ell$  system. Thus, the inner zone of case 1 is sized to contain only 11.355  $\ell$

of unborated water. The outer zone of the base case model is the remaining inventory of burned core-averaged fuel with the design pellet diameter. Any other outer zone characterization was considered

unnecessarily conservative based on the available core data and latest accident scenario.

The other cases in Table XI were done prior to or concurrent with the base case model analyses to quantify the effect of various assumptions. Case 2 confirmed that 15 l of unborated water in optimum core-averaged fuel would still exceed the calculational limit on  $k_{eff}$ . Likewise, cases 3 to 6 confirmed the need for better characterization of the burned core-averaged fuel. At this point, it was decided to actually perform depletion analysis of batch 1 and 2 fuel rather than conservatively extrapolate from the batch 3 depletion case. Using complete burnup analyses allowed an important decrease in the burned core-average enrichment of  $^{235}\text{U}$  (from an extrapolated 2.32 wt% value to a calculated 2.24 wt% value). Cases 7 and 8 show that using optimum particle sizes in the outer core-average zone would raise  $k_{eff}$  above the allowable calculational limit (0.965) even at the higher boron level (5100 wppm) typically maintained in the coolant system.

Finally, case 9 of Table XI uses a spherical model developed from a conservative mixing scenario that assumes an unborated water jet entering the batch 3 fuel region. The inner zone of the mixing model has 0.946 l of unborated water in burned batch 3 fuel. The next region has 17.45 l of water with 2000 wppm boron to simulate the mixing of the remaining unborated water with water at 4950 wppm boron. The mixing model result shows a 3.6%  $\Delta k$  decrease in reactivity and confirms the large degree of conservatism associated with neglecting mixing in the base case model.

Other conservatisms in the LCSA base case were also investigated via auxiliary analyses. Impurities typical of batch 3 fuel that melted and resolidified were considered in  $k_{eff}$  analysis of material code Z of Table III. The resulting  $k_{eff} = 0.76$  indicates a substantial reactivity decrease provided by the impurities. The stainless steel that occupies a large portion of the LCSA region was also ignored in the base case analysis. The largest piece of steel within the LCSA, the grid forging, was used as the basis for a model developed to assess the reactivity worth of this stainless steel. The grid forging is a steel plate, ~35 cm thick, drilled with ~16.5-cm-diam holes in a lattice as shown in Fig. 6.

A model of the grid forging was developed to perform the stainless steel sensitivity analysis; however, each of the holes was assumed to be only 15.24 cm in diameter. Additionally, the size of the grid forging was assumed to be infinite in the radial direction and 35.5 cm high axially. Each hole was assumed to be filled with an optimum mixture of unborated water and fuel. The fuel used in this case was optimum-sized fuel particles, with an enrichment of 2.32% (material DD of Table III). On the top and bottom of the steel was an infinite thickness of borated water reflector. The results obtained from KENO V.a showed  $k_{eff} = 0.794 \pm$

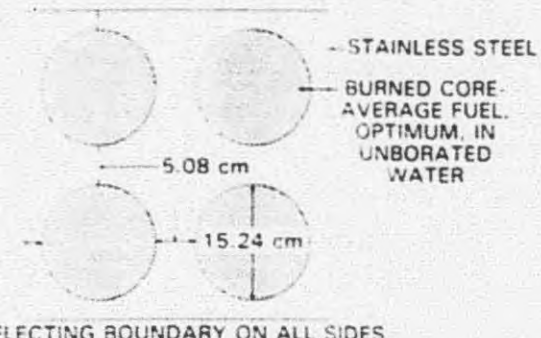


Fig. 6. Criticality safety model considering presence of stainless steel within LCSA.

0.002. This extremely low value of  $k_{eff}$  supports the conclusion that the presence of the stainless steel in the LCSA has a significant negative effect on  $k_{eff}$ .

One interesting facet to the KENO V.a analyses performed for the spherical models of Table XI should be noted. The output from cases 3 through 6 indicates that this particular calculational model causes the source particle distribution to move spatially (or "drift") between generations. In an effort to remedy this problem, cases 1, 7, and 8 were run with twice as many particles per generation. In addition, these cases were also run with XSDRNPM-S. The initial KENO V.a result for case 1 is shown as case 1a of Table XII. The discrepancy between the XSDRNPM-S and KENO V.a results was far beyond that expected based on the standard deviation estimated by KENO V.a. A careful review of both the XSDRNPM-S and KENO V.a analyses showed no apparent problem with either calculation. Thus, nine additional KENO V.a calculations of case 1 were run to obtain a set of ten numerical "measurements" of  $k_{eff}$  from which a mean and variance could be obtained. The results of these ten analyses are shown in Table XII. The mean value obtained from Table XII is reported in Table XI for case 1 and provides excellent agreement with the XSDRNPM-S result.

The conclusion drawn from Table XII is that, for this model, KENO V.a provides a poor estimate of the true standard deviation. The reason for the poor approximation is not clear. It could be tied to the source drift between generations, the fact that the KENO V.a procedure for estimating standard deviation assumes no correlation between generations, or other unknown reasons. The source drift can probably be attributed to the drastic change in the boron level between regions. The very small central region has a high reactivity worth composition. The outer region, which is 600 times larger in volume, has a  $k_{eff}$  that is slightly lower than the system total. Note that previous models that employed adjacent borated and unborated fuel zones such as this were only analyzed with XSDRNPM-S. Since

TABLE XII

Results of Ten KENO V.a Calculations of the Base Case LCSA Model (Case 1) of Table XI

Case*	Effective Multiplication Factors, $k_{eff} \pm \sigma$
1a	$0.9663 \pm 0.0010$
1b	$0.9550 \pm 0.0011$
1c	$0.9612 \pm 0.0011$
1d	$0.9648 \pm 0.0011$
1e	$0.9608 \pm 0.0012$
1f	$0.9574 \pm 0.0013$
1g	$0.9584 \pm 0.0011$
1h	$0.9576 \pm 0.0012$
1i	$0.9566 \pm 0.0011$
1j	$0.9610 \pm 0.0011$
Mean	$0.9559 \pm 0.0011$

Cases differ only in the initial random number. There are 200 000 histories per case.

$$\text{Mean } = \bar{x} = \frac{\sum k_{eff}}{10} = 0.9599$$

Standard deviation of case distribution

$$\sigma = \left[ \frac{\sum (k_{eff} - \bar{x})^2}{9} \right]^{1/2} = 0.0036.$$

Standard deviation of mean =  $\sigma/\sqrt{10} = 0.0011$ .

This work reaffirmed the validity of the XSDRNPMS calculation; there was no reason to review the earlier XSDRNPMS calculations with similar models.

#### Other Tasks

The three application areas described above required the largest amount of analytic support. However, analytic support was also supplied for a variety of smaller tasks. One such set of analyses was performed for the storage containers used to store fuel assembly end fittings at TMI-2. Lack of certainty regarding the amount of fuel accompanying the end fitting in the container necessitated criticality safety analyses. The cylindrical container model is shown in Fig. 7, and the KENO V.a analysis results are shown in Table XIII. In addition, cases with polyethylene moderation were analyzed. The results of the analysis provided adequate confirmation that the containers would be maintained in an adequate subcritical state during normal and abnormal (case 4) storage conditions.

Table XIV provides the critical and limiting fuel mass quantities developed for several unborated water-moderated systems with and without a reflector. The spherical models were analyzed easily by doing automated searches to locate the inner zone radius that pro-

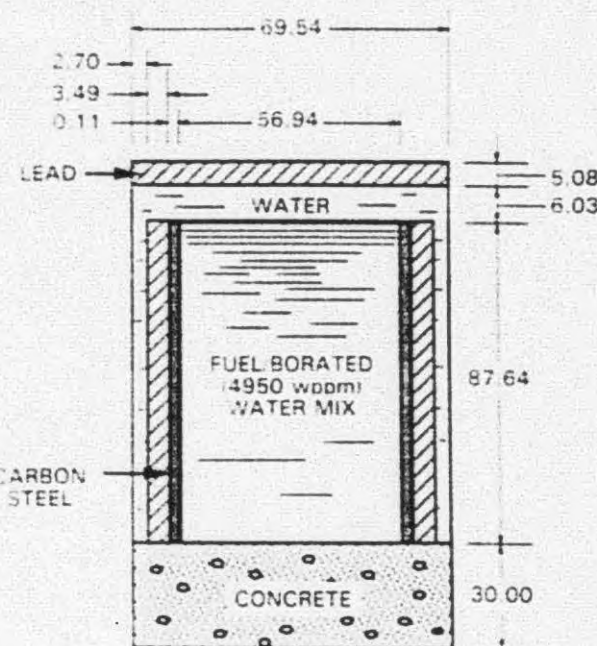


Fig. 7. Criticality safety analysis model for end fittings container. Dimensions are given in centimetres.

TABLE XIII  
Results of Criticality Analyses for  
End Fittings Container

Case	Model Description	Multiplication Factor
1	Single unit	$0.795 \pm 0.003$
2	Single unit, unborated water removed	$0.779 \pm 0.003$
3	Infinite planar array	$0.893 \pm 0.003$
4	Infinite double-height array	$0.933 \pm 0.003$

vided the desired  $k_{eff}$  value. The cylindrical models were analyzed with KENO V.a and required manual iteration of the cylindrical dimensions. The purpose of cases 1 through 7 was to assess the degree of conservatism inherent in the single-parameter safe fuel mass limit of 70 kg utilized at the TMI-2 site. Cases 8 through 11 of Table XIV were done to obtain information on the critical mass limit for core-averaged fuel in unborated water.

#### CONCLUSION

Criticality safety analyses for the TMI-2 defueling operations have been an important part of establishing defueling procedures, maintaining safe operations,

TABLE XIV  
Critical and Limiting Mass Quantities for Fresh Batch 3 and Core-Averaged Fuel

Case	Model	Fuel Material Code* [Outer Radius (cm)]	Steel Liner Thickness (cm)	Water Reflection Thickness (cm)	Multiplication Factor, $k_{eff}$	Fuel Mass (kg)
1	Sphere	C(22.5)	0.3175	30	1.0	137.4
2	Sphere	C(21.6)	0	30	1.0	122.2
3	Cylinder	C(17.0) <sup>b</sup>	0.3175	30	0.990 ± 0.004	178.0
4	Cylinder	C(16.5) <sup>b</sup>	0	30	0.996 ± 0.004	162.8
5	Sphere	C(23.8)	2.54	0	1.0	162.1
6	Sphere	K(24.4)	0.3175	30	1.0	176.1
7	Sphere	K(23.5)	0	30	1.0	163.7
8	Sphere	EE(24.7)	0	30	1.0	182.0
9	Sphere	EE(22.7)	0	30	0.965	141.0
10	Sphere	EE(28.9)	0	0	1.0	292.0
11	Sphere	EE(26.9)	0	0	0.965	235.0

See Table III for fuel material codes.

<sup>b</sup>Cylinder height equal to twice the diameter.

and demonstrating compliance with internal and regulatory safety requirements. The computational tools used for the work are well established within the criticality safety community. A simple bounding approach was taken in developing the calculational models. The use of well-established tools and bounding models enabled rapid response to analysis requests and led to a relatively smooth review process by internal and external reviewers.

#### ACKNOWLEDGMENTS

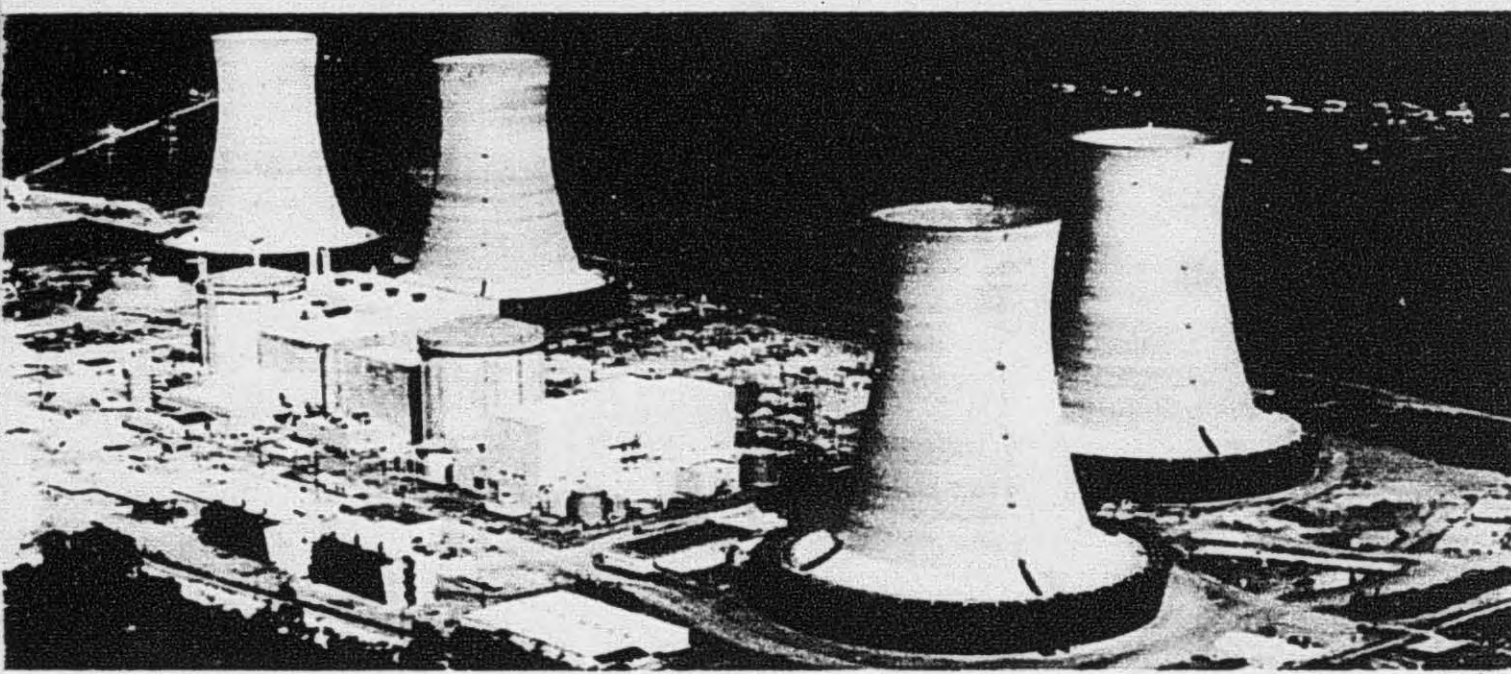
The authors are indebted to J. R. Knight, P. B. Fox, S. P. Cerne, and O. W. Hermann who helped perform many of the calculations reported herein.

#### REFERENCES

1. D. S. WILLIAMS, J. C. ROMMEL, and R. L. MURRAY, "An Overview of Nuclear Criticality Safety Performed to Support TMI-2 Defueling," *Trans. Am. Nucl. Soc.*, **57**, 508 (1988).
2. "SCALE: A Modular Code System for Performing Standardized Computer Analyses for Licensing Evaluation," NUREG/CR-0200, Vols. 1-3, U.S. Nuclear Regulatory Commission (originally issued July 1980, reissued Jan. 1982, Rev. 1 issued July 1982, Rev. 2 issued June 1983, Rev. 3 issued Dec. 1984). Code system available from the Radiation Shielding Information Center at Oak Ridge National Laboratory.
3. N. M. GREENE, L. M. PETRIE, and R. M. WESTFALL, "NITAWL-S: SCALE System Module for Performance Resonance Shielding and Working Library Production," NUREG/CR-0200, Rev. 3, Sec. F2, U.S. Nuclear Regulatory Commission (Dec. 1984).
4. L. M. PETRIE and N. F. LANDERS, "KENO V.a: An Improved Monte Carlo Criticality Program with Super-Grouping," NUREG/CR-0200, Rev. 3, Sec. F11, U.S. Nuclear Regulatory Commission (Dec. 1984).
5. N. M. GREENE and L. M. PETRIE, "XSDRNPM-S: A One-Dimensional Discrete Ordinates Program for Transport Analysis," NUREG/CR-0200, Rev. 3, Sec. F3, U.S. Nuclear Regulatory Commission (Dec. 1984).
6. O. W. HERMANN and R. M. WESTFALL, "ORIGEN-S: SCALE System Module to Calculate Fuel Depletion, Actinide Transmutation, Fission Product Buildup and Decay, and Associated Radiation Source Terms," NUREG/CR-0200, Rev. 3, Sec. F7, U.S. Nuclear Regulatory Commission (Dec. 1984).
7. M. J. BELL, "ORIGEN - The ORNL Isotope Generation and Depletion Code," ORNL-4628, Oak Ridge National Laboratory (May 1973).
8. N. F. LANDERS and L. M. PETRIE, "CSAS4: An Enhanced Criticality Safety Analysis Module with an Optimum Pitch Search Option," NUREG/CR-0200, Rev. 3, Sec. C4, U.S. Nuclear Regulatory Commission (Dec. 1984).
9. O. W. HERMANN, "SAS2: A Coupled One-Dimensional Depletion and Shielding Analysis Code," NUREG/CR-0200, Rev. 3, Sec. S2, U.S. Nuclear Regulatory Commission (Dec. 1984).
10. J. R. KNIGHT, "SUPERDAN: Computer Program for Calculating the Dancoff Factor of Spheres, Cylinders, and

- Slabs," ORNL/NUREG/CSD/TM-2, Oak Ridge National Laboratory (1978).
11. N. M. GREENE, J. L. LUCIUS, L. M. PETRIE, W. E. FORD III, J. E. WHITE, and R. Q. WRIGHT, "AMPX: A Modular Code System for Generating Coupled Multi-group Neutron-Gamma Libraries from ENDF/B," ORNL/TM-3706, Oak Ridge National Laboratory (Mar. 1976).
  12. R. M. WESTFALL and J. R. KNIGHT, "SCALE System Cross Section Validation with Shipping-Cask Critical Experiments," *Trans. Am. Nucl. Soc.*, 33, 368 (1979).
  13. L. M. PETRIE and J. T. THOMAS, "Assessment of Computational Performance in Nuclear Criticality," ORNL/CSD/TM-224, Oak Ridge National Laboratory (Jan. 1985).
  14. R. L. MURRAY, Consultant to D. S. Williams, Bechtel North American Power Corporation, "Selection of Critical Experiments," Letter Report (Apr. 5, 1984).
  15. T. C. ENGELDER, N. L. SNIDOW, R. H. CLARK, C. E. BARKSDALE, R. H. LEWIS, and M. N. BALDWIN, "Spectral Shift Control Reactor Basic Physics Program, Critical Experiments on Lattices Moderated by D-O-H-O Mixtures," BAW-1231, Babcock & Wilcox Company (Dec. 31, 1961).
  16. A. R. BOYNTON, Q. L. BAIRD, K. B. PLUMLEE, W. C. REDMAN, W. R. ROBINSON, and G. S. STAN-
  - FORD, "High Conversion Critical Experiments," ANL-7203, Argonne National Laboratory (Jan. 1967).
  17. G. S. HOOVLER, M. N. BALDWIN, E. L. MACEDA, and F. G. WELFARE, "Critical Experiments Supporting Underwater Storage of Tightly Packed Configurations of Fuel Pins," BAW-1645-4, Babcock & Wilcox Company (Nov. 1981).
  18. R. M. WESTFALL, J. R. KNIGHT, P. B. FOX, O. W. HERMANN, and J. C. TURNER, "TMI-2 Criticality Studies: Lower-Vessel Rubble and Analytical Benchmarking," ORNL/CSD/TM-222, Oak Ridge National Laboratory (Dec. 1985).
  19. R. M. WESTFALL, J. T. WEST, G. E. WHITESIDES, and J. T. THOMAS, "Criticality Analyses of Disrupted Core Models of Three Mile Island Unit 2," ORNL/CSD/TM-106, Oak Ridge National Laboratory (1979).
  20. H. M. CUNDY and A. P. ROLLETT, *Mathematical Models*, Oxford University Press, New York (1961).
  21. W. C. JORDAN, C. V. PARKS, and L. M. PETRIE, "An Improved Dancott Correction Factor for the SCALE Code System," *Trans. Am. Nucl. Soc.*, 56, 324 (1988).
  22. J. F. BRIESMEISTER, Ed., "MCNP - A General Monte Carlo Code for Neutron and Photon Transport, Version 3A," LA-7396-M, Rev. 2, Los Alamos National Laboratory (Sep. 1986).

May 1985



This is an informal report intended for use as a preliminary or working document.

# GEND

General Public Utilities • Electric Power Research Institute • U.S. Nuclear Regulatory Commission • U.S. Department of Energy

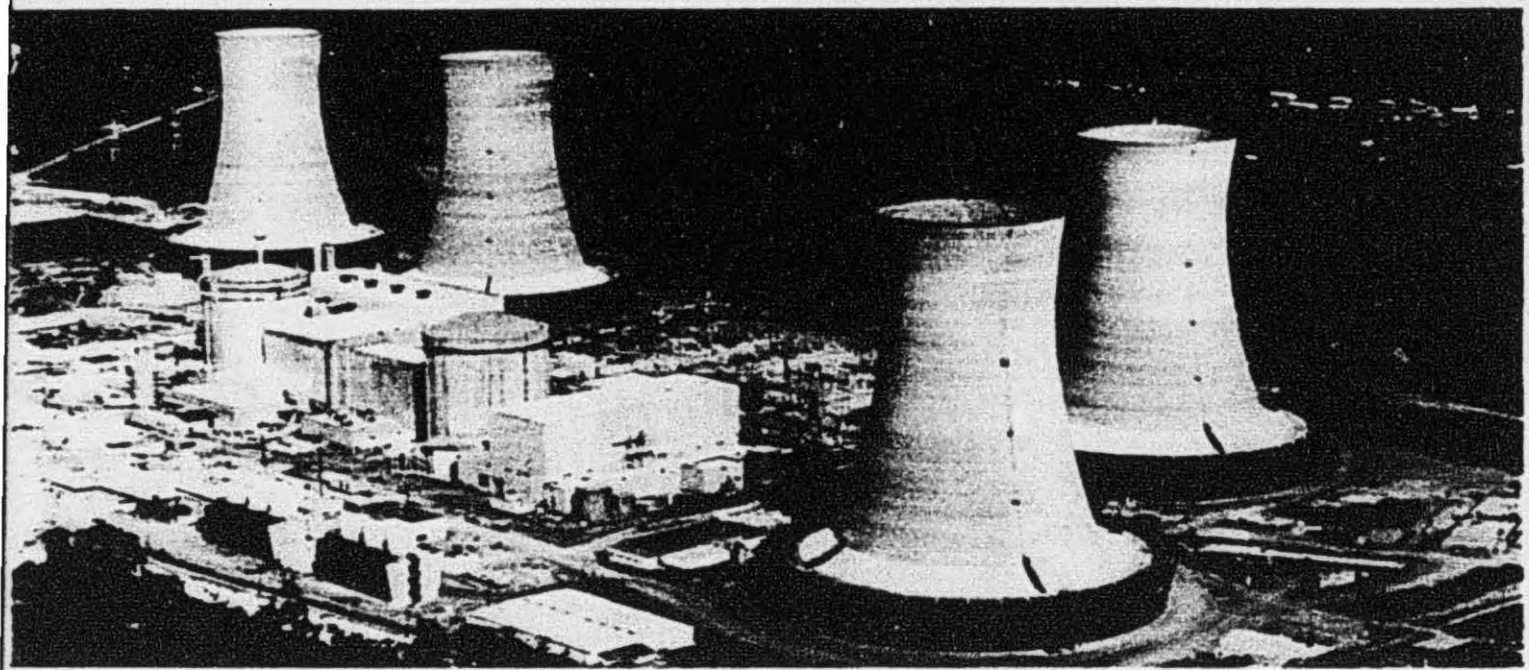
## TMI-2 H8A CORE DEBRIS SAMPLE EXAMINATION FINAL REPORT

George O. Hayner

Prepared for the  
U.S. Department of Energy  
Three Mile Island Operations Office  
Under Contract No. DE-AC07-76ID01570

9304150048 930408  
PDR ADOCK 05000320  
PDR  
P

June 1989



This is an informal report intended for use as a preliminary or working document.

# GEND

General Public Utilities • Electric Power Research Institute • U.S. Nuclear Regulatory Commission • U.S. Department of Energy

## TMI-2 B-LOOP STEAM GENERATOR TUBE SHEET LOOSE DEBRIS EXAMINATION AND ANALYSIS

T. L. Hardt  
G.O. Hayner

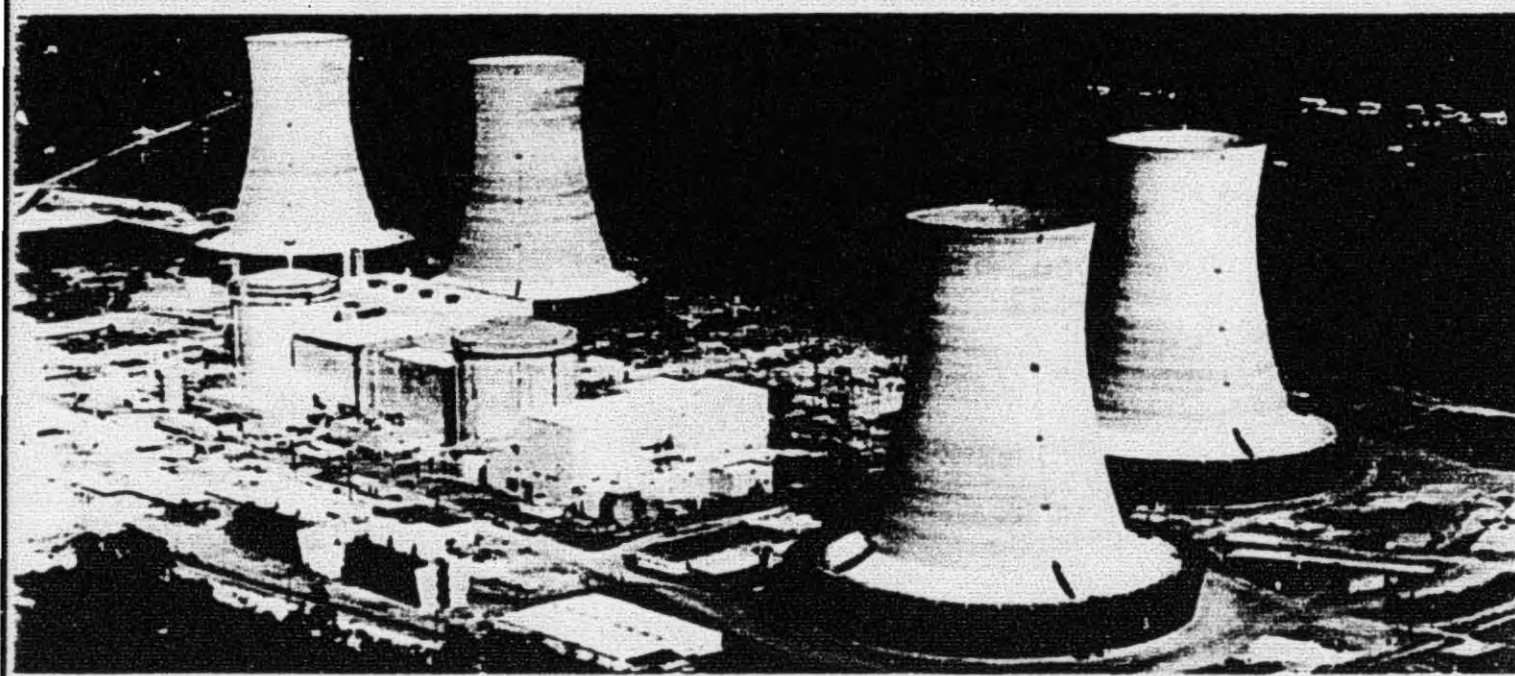
Prepared for the  
U.S. Department of Energy  
Three Mile Island Operations Office  
Under Contract No. DE-AC07-76ID01570

9304150050 930408  
PDR ADDCK 05000320  
PDR  
P

GEND INF 075 Part 1

**GEND-INF- 075**

September 1986



This is an informal report intended for use as a preliminary or working document

# **GEND**

General Public Utilities • Electric Power Research Institute • U.S. Nuclear Regulatory Commission • U.S. Department of Energy

TMI-2 CORE DEBRIS GRAB SAMPLES--

EXAMINATION AND ANALYSIS

PART 1

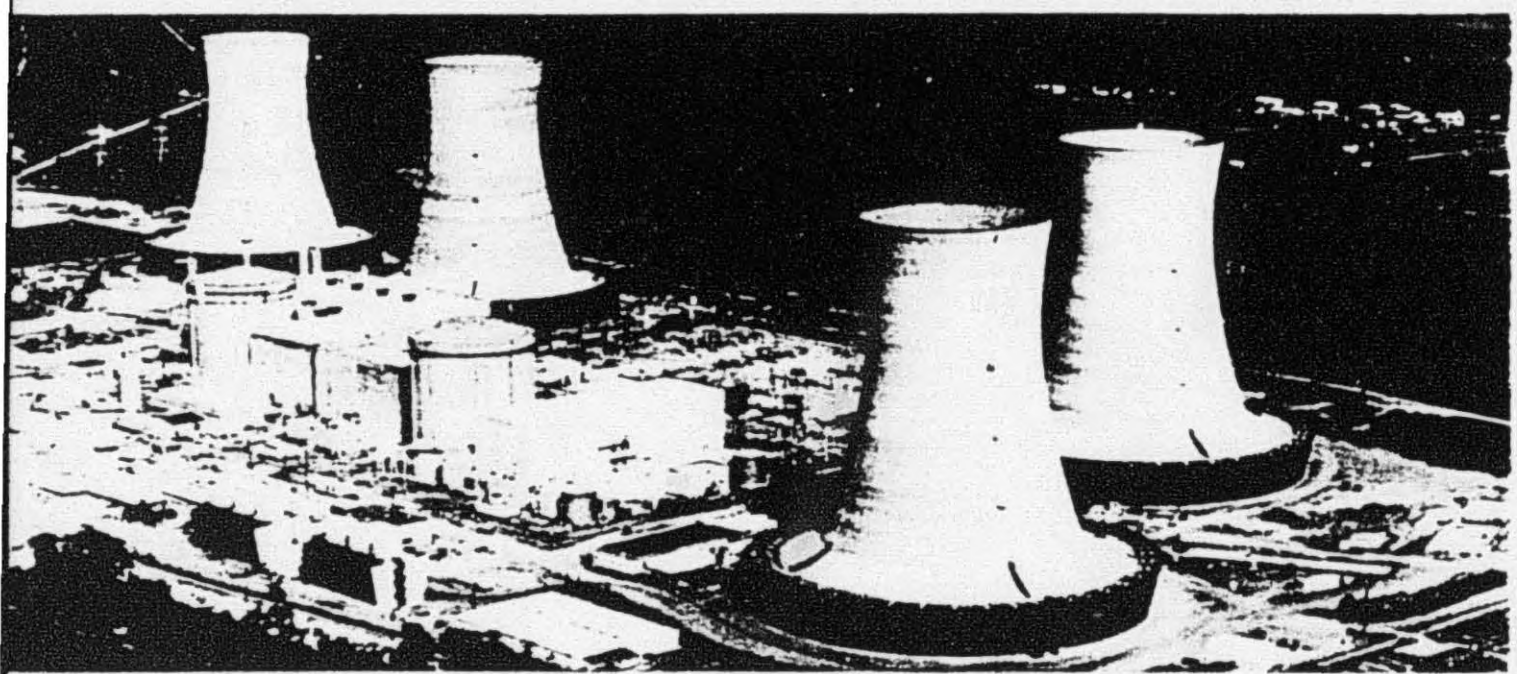
GPU SYSTEM LIBRARIES  
TMI

D. W. Akers  
E. R. Carlson  
B. A. Cook

S. A. Ploger  
J. O. Carlson

Prepared for the  
U.S. Department of Energy  
Three Mile Island Operations Office  
Under Contract No. DE-AC07-76ID01570

9304150052 93040B  
PDR ADOCK 05000320  
P PDR



This is an informal report intended for use as a preliminary or working document.

# GEND

General Public Utilities • Electric Power Research Institute • U.S. Nuclear Regulatory Commission • U.S. Department of Energy

## TMI-2 CORE DEBRIS GRAB SAMPLES--

### EXAMINATION AND ANALYSIS

#### PART 2

D. W. Akers  
E. R. Carlson  
B. A. Cook

S. A. Ploger  
J. O. Carlson

Prepared for the  
U.S. Department of Energy  
Three Mile Island Operations Office  
Under Contract No. DE-AC07-76ID01570